POLITECNICO DI MILANO

School of Civil, Environmental and Land Management Engineering

Master of Science in Civil Engineering for Risk Mitigation

PHYSICALLY BASED NUMERICAL SOIL EROSION MODEL

Thesis Supervisors : Prof. Luca BONAVENTURA, Prof. Laura Longoni
Thesis Co-supervisor : Dr. Davide BRAMBILLA

Master of Science Thesis of:

Jeremi Kazimierz GRUDNICKI Matr. 849799

Academic Year 2017–2018

Contents

1 Introduction **9**

2 Erosion **11**

2.1 Definition and classification of erosion 11

2.1.1 Aeolian erosion 11

2.1.2 Water - rainfall and surface runoff erosion 14

2.1.3 Water - coastal erosion 17

2.1.4 Water - river erosion 20

3 Review of models **25**

3.1 Classification of erosion models 25

3.2 Empirical models 26

3.2.1 Universal Soil Loss Equation - USLE 27

3.2.2 Revised Universal Soil Loss Equation - RUSLE 30

3.2.3 Erosion Potential Method - Gavrilovic Method 32

3.3 Concpetual models 35

3.3.1 Agricultural Non-Point Source Pollution Model - AGNPS 36

3.3.2 Simulator for Water Resources in Rural Basins - SWRRB 38

3.3.3 Large Scale Catchment Model - LASCAM 38

3.4 Physically based models 40

3.4.1 Limburg Soil Erosion Model - LISEM 40

3.4.2 Water Erosion Prediction Project - WEPP 42

3.4.3 European Soil Erosion Model - EUROSEM 44

4 Model equations **47**
4.1 Model equations 48
4.2 Discretization approach 54

5 Preliminary tests **59**
5.1 Plane surface 59
5.1.1 Test 1.1 - Impermeable surface 59
5.1.2 Test 1.2 - Movement between layers 61
5.1.3 Test 1.3 - Run-off infiltration 64
5.1.4 Test 1.4 - Only surface runoff with a fine mesh 66
5.1.5 Test 1.5 - Fine mesh and a longer simulation 66
5.1.6 Test 1.6 - Runoff infiltration with a fine mesh 68
5.1.7 Test 1.7 - Runoff infiltration with a fine mesh and a longer simulation time 69
5.1.8 Test 1.8 - Sediment transportation 72
5.2 Paraboloidal surface 73
5.2.1 Test 2.1 - Impermeable surface 73
5.2.2 Test 2.2 - Movement between layers 76
5.2.3 Test 2.3 - Runoff infiltration 77
5.2.4 Test 2.4 - Mesh refinement and sediment transportation 78
5.2.5 Test 2.5 - Rain as initial condition 80

6 Realistic test **83**
6.1 Area of study 83
6.1.1 Test 3.1 and 3.2 - Uniform rain on the whole domain with rough and fine mesh 86
6.1.2 Test 3.3 and 3.4 - Uniform rain over the whole domain with changes in friction parameters 88

7 Conclusion **93**

Bibliography **94**

List of Tables

3.1 Gavrilovic descriptive factors reference values 34
3.2 LASCAM input and output 39

5.1 Test 1.1 parameters 60
5.2 Test 1.2 parameters 62
5.3 Test 1.3 parameters 64
5.4 Test 1.5 parameters 66
5.5 Test 1.6 parameters 69
5.6 Test 2.1 parameters 74
5.7 Test 1.2 parameters 76

6.1 Simulation parameters 87
6.2 Simulation parameters 88

List of Figures

2.1 Example of deflation (left) and abrasion (right) 12
2.2 Example of sandsheet (left) and ripple (right) 13
2.3 Example of a desert dune 13
2.4 Sheet erosion with rills forming in the background(left) and a stabilizing geosynthetic (right) 15
2.5 A clearly visible rill in the field 16
2.6 Gullies 17
2.7 Coastal erosion consequences 19
2.8 A stony seawall 19
2.9 The Hjulstrom curvel 21
2.10 Concrete-Lined Channel 21
2.11 A riprap 22
2.12 Riverbank protected with gabions 23
2.13 A checkdam (left) and a drop (right) 23

3.1 An example of contour tillage 29
3.2 An output example of LISEM. Source:[51] 42

4.1 Domains' schematics 48

5.1 Orography (left) and initial condition (right) 60
5.2 Test 1.1 results - final water height (left) and velocity field (right) after time T=24h 61
5.3 Initial condition 62
5.4 Test 1.2 results after time T=120h 63

5.5 Test 1.3 results after time T=120h 65
5.6 Test 1.4 results - rough mesh (left) and fine mesh (right) . . . 67
5.7 Test 1.5 results 68
5.8 Test 1.6 results 70
5.9 Test 1.7 results 71
5.10 Test 1.8 results (T=24h) 72
5.11 Orography in second set of tests 73
5.12 Initial condition 74
5.13 Test 2.1 results - after time T=72h 75
5.14 Test 2.2 Initial condition 76
5.15 Test 2.2 results after time T=72h 77
5.16 Test 2.3 orography and initial condition 78
5.17 Test 2.3 results after time T=72h 79
5.18 Test 2.4 results (left, rough mesh) and fine mesh results (right) 81
5.19 Test 2.5 results after T=72h 82

6.1 Location of Tartano 84
6.2 A view of Val Lunga 84
6.3 Look at Val Tartano 85
6.4 Morphology of the valley 86
6.5 Test 3.1 and 3.2 results after T=30 days. 40x40m mesh (left) and 60x60m mesh (right). 90
6.6 Test 3.3 and 3.4 results after T=10 days. $d_{90} = 0.2m$ (left) and $d_{90} = 0.05m$ (right). 91

Chapter 1

Introduction

Soil erosion is a phenomenon present in all regions of the world. It is a threat both to human beings and the natural environment. The need to mitigate the negative effects of erosion has become urgent in the beginning of the XX century. Since then, scientist have been developing models to help understand the factors that influence erosion and the processes related to it. Some of these models were purely empirical - relying on statistical relationships between the values measured in field and the soil sediment yield. Other tried to describe the physical processes by means of mathematical equations like mass conservation laws or laws describing movement of water.

This thesis is a part of this development and improvement in the field of erosion modelling. It introduces and tests a physically based numerical erosion model based on conservation laws. To assess the usefulness of the model, it has been tested on idealized configurations and on a realistic orography of Val Tartano. Apart from that, in this thesis, erosion phenomenon will be classified and described. Also brief review of models is included - classification, assumptions and application of currently used erosion models are included.

The tested model will be also described to explain the methodology that was adopted in it. Both the conceptual division of soil into separate layers and the discretization of conservation laws will be provided. The conclusions drawn from the work done will be included in the final chapter of the thesis.

Chapter 2

Erosion phenomena

2.1 Definition and classification of erosion

Erosion is a process of removal of soil and transporting it to a different location. This is done due to actions of so called "erosive agents". These agents are water (flowing water or rain), wind or ice. After being eroded, soil is transported away either in a form of bed load or suspended load in streams or carried away by the wind (a sandstorm is an example of that process). Soil or rock material can be also dissolved in water and, due to changed physical conditions, deposited in a different location.

2.1.1 Aeolian erosion

This type of erosion is caused by wind, which may act in two ways[21]. First is called deflation - when a loosened, fine material is picked up by the blowing wind from the ground and carried away. Second type is abrasion - it is mechanical wear of cohesive material. Which process is dominating is dependant on the properties of the soil. Deflation is the most evident in desert environment, where lack of vegetation facilitates the action of wind on sand particles. Abrasion's distinctive effects are rocks eroded in irregular shapes. Wind can carry away soil particles in three ways. Particles smaller than 0.2 mm can be transported in suspension. The travel distance in this case can be very long, winds blowing from Africa are able to transport dust

across the Mediterranean Sea and deposit them in Italy. Bigger grains, up to 1 cm in size, are moving in the form of saltation, they are too heavy to be carried in air, so they are skipping and bouncing along the terrain surface. The biggest particles susceptible to aeolian erosion are being pushed along the surface without loosing contact with the ground - it is called creeping. In zones, where wind gets weaker, deposition occurs. Characteristic forms of

Figure 2.1: Example of deflation (left) and abrasion (right)

deposition of aeolic material are dunes, ripples and sand sheets. Sand sheets form if the wind is too weak to form a dune. They are flat areas covered more or less uniformly by the deposited soil. Ripples are crests and troughs left on soil surface that are perpendicular to the wind direction. However, the most iconic form of aeolian deposition are dunes. They are hills of loose sand that come in different shapes and sizes, but are usually longer and milder on windward side and shorter and steeper on the opposite side. The beginning of formation of a dune is sand that, being dragged by wind, stops at obstacles like boulders, dense vegetation or small hills. Continuous process of deposition in these areas eventually form a dune.

Wind erosion might be very harmful when acting on agricultural areas. It carries away the finer, more chemically active components of the soil, which very often contain nutrients for plants [55]. This puts in jeopardy farming activities, to which fertility of soil is a crucial factor. Another problem is connected to deposition. Nordstrom and Hotta [41] say that dust brought by wind is equally as harmful. From the point of view of farming, it buries the plants and blocks sunlight. From hydrologic perspective - it clogs streams

Figure 2.2: Example of sandsheet (left) and ripple (right)

Figure 2.3: Example of a desert dune

and drainage channels, muddies waters and pollutes water systems. Finally, it is also harmful to people - exposition to aeolic particles suspended in the wind causes skin and eye irritations and may lead to serious respiratory diseases. So far, the only feasible method of mitigation of this type of erosion is planting new vegetation. This is done on big scale for example in areas that suffered fires [36], however the effectiveness and efficiency of this method is still a subject of research.

2.1.2 Water - rainfall and surface runoff erosion

Water is one of the main erosive agents. Sheet, rill and gully erosion is the result of rain. Raindrops impacts make soil more loose and make the soil particles available for transportation by runoff. Runoff forms, when the rate of infiltration is lower than the rainfall intensity and some water is left on the surface. Rate of this kind of erosion depends mainly on:

- Erosivity - that is the rainfall intensity and duration
- Erodibility - which depends on the physical and mechanical characteristics of soil
- Slope length - longer slopes promote erosion, as the slope becomes longer, water running down becomes deeper
- Slope steepness - the steeper the slope is, the faster the runoff flows and the more energy it has to carry away soil particles

Firstly, water erosion takes the form of **sheet erosion**. It can be described as a removal of soil particles, detached previously by raindrop impact, by runoff in the form sheet. As a result, a layer of approximately constant thickness is removed from the area. It results in a loss of very precious fertile topsoil. One of the most prone to that erosion types of surfaces are recently ploughed fields in which the soil is very poorly consolidated. Sheet erosion may be mitigated by the presence of vegetation, which acts as a stabilizer of pore spaces in soil. Another way is to consolidate soil with geotextiles or geocrates. Generally it is difficult to measure the rates of sheet erosion only, as it quickly transforms

into rills after a couple of hours of rain. However, Bodoque et al. [8] proposed a method that was based on dendrogeomorphological analysis of exposed tree roots. Testing this method in Central Spain they obtained results of 29-44 t/ha/year on one site and 19-31 t/ha/year on the other.

Figure 2.4: Sheet erosion with rills forming in the background(left) and a stabilizing geosynthetic (right)

The next step of water erosion process is the **rill erosion**. Rills are shallow channels which are formed along the slope. Their depth is usually of the order of tens of centimetres. Smaller channels, which depth is of the order of centimetres are called microrills. Rills form, as the shear forces of flowing water overcomes the resistance of the soil. These shear forces can be described by a parameter called shear velocity [46]:

$$u_t = \sqrt{GRS} \tag{2.1}$$

where:
G - gravitational acceleration
R - hydraulic radius of the flow
S - slope (sine of the slope angle)

The main factors governing the resistance of soil is the surface roughness and the soil shear strength. The latter can be measured by in-situ tests, for example the vane shear test or the torsional shear box. Surface roughness is composed by many elements - tillage marks, topsoil aggregates, vegetation cove, mulches. The total force that opposes the flow is therefore composed of

the resistance of soil particles and the resistance of macro-roughness elements [46]. The mitigation methods are essentially the same as in the sheet erosion.

Figure 2.5: A clearly visible rill in the field

When many rills join together to form bigger channels, it can be stated that the **gully** erosion has started. Gullies are channels that can extend to tens of meters, both in width as in depth. Apart from rill-joining, another possible mechanism of gully creation is an unusually big flow in a watercourse. Such a flow may erode the banks and the riverbed. The banks of a gully may also collapse, increasing the overall width. A condition that highly promotes the formation of gullies is the runoff concentration. Any furrows, fences, tracks or field roads are the potential places of gully formation. This is why a wise property management must be employed in order to cause minimal runoff concentration. Poesen et al. [45] put a lot of stress on the role of vegetation in controlling gully erosion. They explain that the resistance to gully erosion of a vegetation with well-developed root-mats may be of the same order as the underlying bedrock.

Some models are capable of predicting gully erosion. These are CREAMS, GLEAMS, EGEM and WEPP [45], however their performance in that matter has not been yet thoroughly tested. Martinez-Casasnovas [34] has used the possibilities of GIS, DEM and remote sensing to map and quantify gully erosion. He was able to measure gully deepening and in his research zone in

Catalonia, Spain he computed that gullies eroded 1322 t/ha/year.

Gullies change the landscape substantially - they can threaten buildings stability or make an agricultural field completely unusable. Also the big amount of soil that is being eroded can clog waterways or pollute aquifers. This is the most dangerous and problematic form of erosion. While sheet and rill erosion mainly cause problems from the agricultural point of view, gullies pose a real threat to human property and human life.

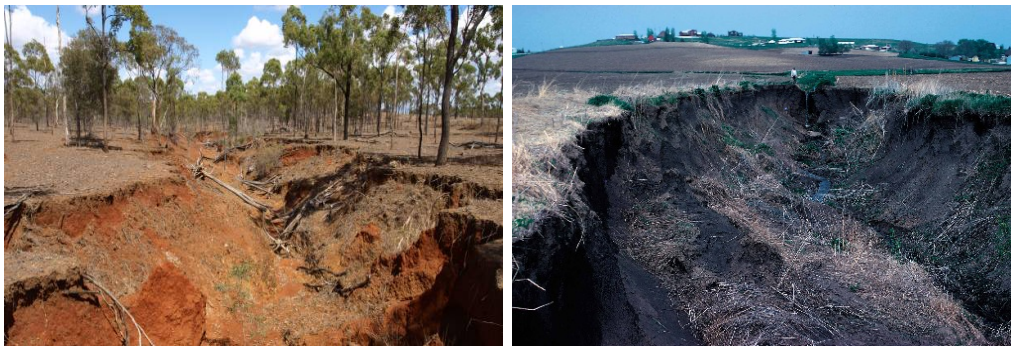

Figure 2.6: Gullies

2.1.3 Water - coastal erosion

Coastal erosion can be described as a process of wearing away beaches and bluffs along coastlines. It is the result of storms, floods, strong waves or of bigger scale processes like lack of sediment supply or sea level rise. It is estimated, that about 70% of sandy beaches worldwide have experienced erosion, but locally, this number can be even higher (86% for U.S. East Coast)[27]. There are four main processes that take place during coastal erosion:

- Hydraulic action - as a result of a wave impact on rock face, the air trapped inside joints is compressed and provokes pressure and stress on the rock itself. It leads to cracks and weakening of the rock mass.

- Abrasion - sand, rock pebbles and debris carried by sea is thrown and smashed against the cliff.

- Solution - it occurs when the cliff is made of dissoluble rocks, for example limestone. Chemicals present in seawater react with rock and dissolves it.

- Attrition - rock pieces in waves collide into each other making themselves smaller, rounder and smoother.

The rate of coastal erosion depends on characteristics of the sea and the shore. In the first group the most important is the wave type. Most destructive are those waves that are high (relatively to the length). They have a strong backwash, which carries away soil particles deeper into the sea. The chemical composition of seawater is also important, especially for coasts prone to solution. Amongst shore characteristics, the most important is the type of rock and the morphology of the cliff. Stronger rocks like basalt or granite are a lot more resistant than limestone, shale and clay. Also the more fractures rock mass has, the lower is its resistance to the hydraulic action. From morphological point of view, steeper cliffs are more susceptible to erosion than milder ones. Steep cliff is more likely to loose stability in case of erosion of its foot. Apart from that, human activity can also favour the process. Buildings on cliff tops are sources of additional stress on the rock and the construction process itself introduces disturbance in form of vibrations and dynamic load. Studies have shown that the accelerating climate change has also negative impact on the coastal erosion. Zhang et al. [27] indicated that there is a connection between the sea rise level and the erosion of sandy beaches. What is worse, this dependence is highly multiplicative. Leatherman et al. [31] reported that sea level rise of 10cm can result in 15m of shoreline retreat, meaning that the factor is equal to 150.

Protection against coastal erosion has been traditionally done in forms of seawalls and levees. Lately, there has been a growing acceptance of the fact that they bring equally as many disadvantages as advantages. They are expensive to build, need regular maintenance, disturb the natural environment and create a false sense of security. Another possibility may be beach nourishment. It is a process of rebuilding beach by transporting and placing sand from another location. Building artificial dunes is also a solution, however it

Figure 2.7: Coastal erosion consequences

requires a thorough analysis, as they alter the natural habitat and may harm sea and land fauna that live on beaches.

Figure 2.8: A stony seawall

There have been efforts to observe and understand the coastal erosion in different parts of the world. Chen and Zong [14] analysed the development of Changjiang Deltaic shoreline in the area of Shanghai, China. They have pointed out, that dams built in the upstream of river Changjiang stop the sediment from reaching the shore and diminish the size of the river delta.

Mars and Houseknecht [33], by analysing Landsat thematic maps of Alaska coast near the Techekpuk Lake estimated the land loss to coastal erosion to be 1.08 km^2/year in years 1985-2005. Thampanya et al. [57] conducted research in th Gulf of Thailand and computed that the land loss is of order of 0.25 km^2/year to 0.91 km^2/year along the shoreline. Similar order of magnitude was reported by Lantuit and Pollard [29] for Hershel Island in Canada. They estimated 0.45 km^2/year of land loss in the period of 1970-2000.

2.1.4 Water - river erosion

River erosion may be divided into two types - bed erosion and bank erosion. Bed erosion, also called scour, is a process of deepening the valley and occurs when the gradient of the river is steep. Bank erosion, on the other hand, is the broadening of the valley and it happens when the gradient is becoming milder. After a certain point, when the slope is mild, erosion processes stop and eroded material is deposited downstream. The rate of river erosion depends highly on the discharge and velocity. The bigger the discharge, the more sediment can be transported by the stream. The bigger the velocity, the more kinetic energy the stream has and the bigger particles can be eroded. This is why the fastest erosion takes place during floods or in periods of high precipitation. The following diagram presents the relationship between the river velocity and the process taking place with respect to the particle size. It is known as the Hjulstrom curve.

The interaction between the stream and soil in this case can be described by the same four processes already described in coastal erosion - hydraulic action, attrition, solution and abrasion.

River erosion is not necessarily a negative phenomenon. It can lead to formation of floodplains and help agriculture. However, wild, uncontrolled erosion might be also a reason to concern and may require mitigation measures.

The first group of these measures are the ones aimed at increasing erosion resistance of river banks. They increase the critical shear stress that needs to by surpassed by the channel. Channels might by lined in concrete,

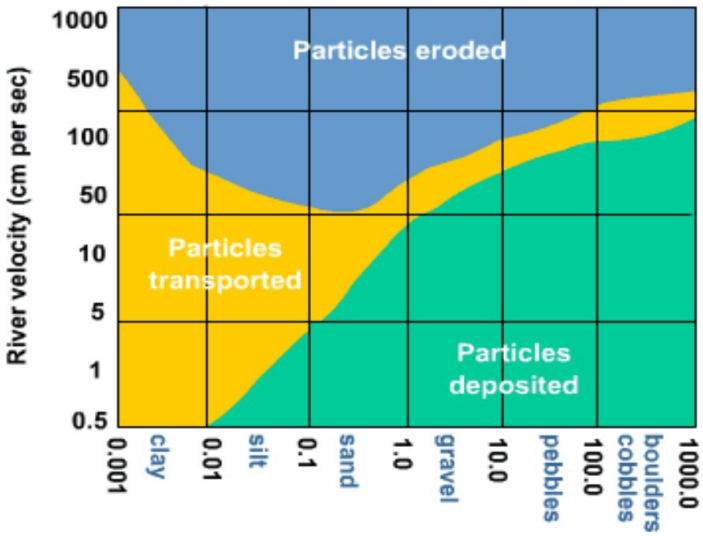

Figure 2.9: The Hjulstrom curvel

which is a permanent and effective solution that requires little maintenance. The drawback is that it is a high alteration of natural habitat and has low aesthetic value. It also favours higher peak flows during possible flooding. A

Figure 2.10: Concrete-Lined Channel

similar solution are rock ripraps. They are made of loose rocks and stones

placed along the channel bound together with a mortar. The durability of such a measure is lower than concrete lining, but it is also cheaper and is better suited in natural environment. An alternative to those two are gabions.

Figure 2.11: A riprap

They are walls made of wire baskets filled with rock. They require more maintenance, as streams in times of elevated peak flows may carry debris, which, thrown against a gabion can damage the basket. Feasibility analysis must be done if gabions are to be constructed in the area of frequent flooding.

There is also a more natural solution - vegetation planted on the channel banks. Plants are progressively higher the further from the stream they are. It is important that the plants need to be compatible with the natural habitat. Their roots go deep into soil and help consolidating it thus resisting erosion.

The second group of mitigation measures aims at reducing the erosion by controlling the river flow. These structures dissipate kinetic energy of streams (slowing them) thus reducing the erosive potential. One of the most popular representatives of this group are check dams. They are built in order to pond water, increase the cross-sectional area and reduce the velocity of

Figure 2.12: Riverbank protected with gabions

the flow. They require regular cleaning upstream, as the slow stream will tend to deposit sediments. Also the riverbed directly in front of the dam needs to be protected to avoid scour. The other example of this measure are drop structures. They may take a form of series of steps which create kind of "micro-waterfalls". Drops are suitable in cases of steep streams with high erosive potential. Like all other structural measures, their drawback is the invasive impact on the natural environment.

Figure 2.13: A checkdam (left) and a drop (right)

River erosion may be monitored by empirical measurements in the field or by more sophisticated methods. Example of the first can be found in work

of Lawler et al. [30]. The idea was to read the bank retreat rate from pins made of silicon bronze welding rode. These pins were organized into grids on each side of the river. 11 sites were along 130km of Swale-Ouse river and gathered data over 14 and a half months every 18-30 days. These empirical observations were in accordance to the expected results - erosion was quicker in the areas of increased discharge and erodible soils. Rate of bank retreat varied from 82 to 440mm over the whole study period.

River bank erosion can be also studied using GIS techniques. Using this technology, a probability of erosion may be assessed using physical data. Governing factors are the distance from the active stream, values characterising stream (peak flow) and values representing morphology and natural environment of the area (sediment type, vegetation). This method was employed by Winterbottom and Gilevar on river Tummel in Scotland [59]. They point out that employing GIS makes the whole analysis a lot more time effective and more precise thanks to refinement of the spatial discretization. This approach may be used to quickly identify areas prone to erosion and improve river management. However, applicability depends on availability of the data.

Described problem may be also approached purely numerically. Nagata et al. [40] proposed a model that investigates bed and bank deformation in 2D. The model is based on continuity and momentum balance equations. It takes into account bed scouring, bank collapse, deposition of the collapsed material and transportation of the deposited material. The authors successfully tested the model on channels in laboratory conditions. This indicates that it might be also applied to real case scenarios.

Chapter 3

Review of currently used erosion models

3.1 Classification of erosion models

Nowadays, a high variety of rainfall-runoff and sediment transport simulation models exist. Amongst those in use, three general groups may be distinguished:

- Empirical models
- Conceptual models
- Physically based models

As Merritt et al. [35] point out, some models may combine the elements characteristic for more than one group. For example rainfall-runoff component may be conceptual while sediment transport might be described empirically. Every model requires a different set of input and each provides different output. This implies that there is no simple "best model" and the choice of suitable one depends on the available data, characteristics of the study area and the information that needs to be obtained. Following questions must be answered in order to select the most appropriate method of assessment of soil erosion:

- What data does the model require?
- Is the data reliable and accurate?
- What is the temporal and spatial scale of my study problem?
- What are the computational requirements of the model?
- How precise information do I need to acquire?

Generally, every model must be applied with caution. A lot of models require a calibration and confrontation with the measured values before a confident application in the future. The example here might be the Gavrilovic method. It was developed in Serbia, but a vast amount of studies were performed in order to validate it in other regions of the world, amongst which was Brazil [17], Iran, Italy, Chile [20] and other.

3.2 Empirical models

Empirical models link, by mathematical equations, the effect of erosion process (amount of soil detached) to parameters that can be either objectively measured (temperature, slope gradient, area of basin etc.) or need to be subjectively assigned (soil erodibility factor etc.). These models do not seek to understand the physics of the processes that take place in catchments. Empirical models assume homogeneity of input data throughout the basin. That is the reason why they give more reliable results when applied to limited areas, where the variation of parameters may be considered negligible. Another drawback is the assumption that the data does not change throughout the duration of the analysis which in some cases may be considered unacceptable. In the following sections, three most widely used empirical models will be described: Universal Soil Loss Equation (USLE), Revised Universal Soil Loss Equation (RUSLE), and aforementioned Gavrilovic method also called Erosion Potential Method (EPM).

3.2.1 Universal Soil Loss Equation - USLE

This method was firstly introduced in the United States of America in 1954 at the National Runoff and Soil Loss Data Center. It was the first method that was suitable to be applied throughout the whole USA, unlike the previous equations, like the Corn Belt equation, which were limited to a couple of neighbouring states. Citing the American Agriculture Handbook: [60] "USLE ia an erosion model designed to predict the long time average soil losses in runoff from specific field areas in specified cropping and management systems". USLE provided at least a correct order of magnitude of soil loss in any agriculture area of the USA, provided that the parameters of the equation could be found. In the beginning, this model was used to determine if the soil loss on farms would extent the tolerance which was set to 1-5 tonnes/acre/year [60]. Successively it was started to be used outside the field of agriculture and outside the US as well.

The soil loss equation is composed of six factors:

$$A = RKLSCP \tag{3.1}$$

where,
A is the computed soil loss per unit area [t/ha y]
R is the rainfall and runoff factor [Mj mm/ha h y]
K is the soil erodibility factor [t h/Mj mm]
L is the geometrical slope length factor [-]
S is the slope steepness factor [-]
C is the cover and management factor [-]
P is the support practice factor [-]

The factors will be now described in more detail.

R - rainfall and runoff factor is the quantification of the impact effect of a raindrop. It also gives information of runoff that is produced by a rainfall

event. The value of R can be obtained from maps in literature [60] or from the empirical formulas. For Europe, mostly used is the following one

$$R = 27.38P^{2.17} \tag{3.2}$$

Where P is the rainfall height with a duration of 6 hours and return period of 2 years. This formula is valid for US units and thus needs recalculation into SI units.

K - soil erodibility factor describes how prone is the soil to be eroded. Direct measurement is difficult, because a soil that is considered less susceptible to erosion may display significant loss if it is situated on a steep slope and vice versa - a prone soil on a gentle slope may appear to be resistant. American Handbook [60] provides values for different soil types based on the loss of soil in a "unit" plot. Methods to compute the K factor are still an object of research and development. Auerswald et al. provided a set of equations that facilitate the computation of K, basing on 20000 soil analyses in Central Europe [6]

L and S - are topographic factors that describe the length and the steepness of the slope. In the beginning, the effect of those factors were studied separately, however it is more convenient to combine them and treat as one value LSs. Assuming a simplification that the slope has a uniform gradient, the following empirical equation has been developed:

$$LS = \left(\frac{\lambda}{72.6}\right)^{m} (65.41 \sin^2\theta + 4.56 \sin\theta + 0.065) \tag{3.3}$$

where:
λ - is the slope length in [ft]
θ - is the angle of slope [rad]
m - is a coefficient equal to 0.5 if slope is 5% or more, 0.4 if slope is between 3.5 and 4.5%, 0.3 if slope is between 1 and 3% and 0.2 on slopes less than 1%

In case where the slope cannot be assumed to have a uniform gradient (it is convex, concave or in any other way complicated) an adjusting coefficient must be applied.

C - is the cover and management factor. It is defined as the ratio of soil loss from land cropped under specified conditions to the corresponding loss from clean-tilled, continuous fallow [60]. It is in fact a reduction coefficient that is based on the type of land use in the study area. The more the erosion is prevented, the lower is the coefficient. It varies from 1 for fallow to 0 for build-up environment like roads and houses.

P - is the support practice factor. It takes into account presence of any measures that are aimed at reducing the erosion rate. The most important measures are contour tillage, strip cropping on the contour and terrace systems. In case of no protection, P takes the value 1. In case of mitigating measures present in the study area P takes values between 0.3 and 1, based on the effectiveness of the measures.

Figure 3.1: An example of contour tillage

Nowadays, USLE is used widely in different countries of the world to

predict erosion. Development of satellite photography and remote sensing allowed the researchers to employ GIS data to determine the values of USLE factors. Study performed for Pinto Lake in California by Boyle et al. shows the degree of correlation between USLE predicted sediment yield and the observed sediment at the rate of 80%[10]. Lee [32] performed soil erosion analysis at Boun, Korea, also using GIS and remote sensing to obtain needed data. He correlated the results of USLE to the available results measured on site and came to a conclusion that the accordance between the two was "satisfactory". These two examples, with many other not mentioned here, show that USLE method is widely used and yields reliable results.

3.2.2 Revised Universal Soil Loss Equation - RUSLE

RUSLE is an updated version of previously described USLE equation. It was introduced by the U.S. Department of Agriculture in 1997 in Agriculture Hanbook Number 703 which superseded Handbook Number 537, which described the usage of USLE. The new version contains analyses of data not available during preparation of the previous handbook, which can serve as a guideline for application of RUSLE in local analyses. It changes the charts, tables and equations in order to provide the users more precise tools to determine the ingredients of RUSLE equation[47]. The form of the equation and the meaning of the erosion factors was kept unchanged:

$$A = RKLSCP \tag{3.4}$$

where,
A is the computed soil loss per unit area [t/ha y]
R is the rainfall and runoff factor [Mj mm/ha h y]
K is the soil erodibility factor [t h/Mj mm]
L is the geometrical slope length factor [-]
S is the slope steepness factor [-]
C is the cover and management factor [-]
P is the support practice factor [-]

Some worth noting changes and innovations included in RUSLE method include[47][48]:

- Computer algorithms to calculate the needed values
- Development of variable K factors
- Guidance for estimating erosion in areas experiencing freeze and thaw phenomenon
- Introduction of sub-factors to compute the C factor which take into consideration previous land use of the area
- Introduction of routines for modelling erosion on rangeland sites
- Coverage of new erosion mitigation practices
- Improvement of modelling on sites undergoing construction, mining and land reclamation
- New algorithms for LS calculation

Sadly, until this moment, RUSLE was not broadly validated in not typical environments - the ones that were previously unreachable for USLE. These are: "sustainable farms", new cropping techniques, construction sites and mining zones. These areas are particularly interesting and research is still needed. There is however, a sizeable amount of research in which RUSLE was used in other zones to predict erosion. Spaeth et al. [54] evaluated soil loss predictive abilities of USLE and RUSLE in rangeland environment of the western USA. Results showed that both methods displayed the same linear patterns, however the magnitude of error for RUSLE was smaller. Also USLE showed more outliers while RUSLE results were scattered in vicinity of the 1:1 (predicted soil loss:measured soil loss) line. Anigma et al. [4] used RUSLE to predict erosion phenomenon for central Kenyan highlands. Results showed 134 [T/ ha y] for LS between 0-10 which was considered reasonable with comparison to 223 [T/ ha y] of measured soil loss for LS factor between 8-12. He also points out that RUSLE helped in identification

of especially erosion prone areas. Lastly, Terranova et al. [56] used RUSLE to predict future threats to Calabria region. Using data extracted from GIS environment and putting them into RUSLE model he developed scenarios in which he takes into consideration deforestation due to fire. The results show that this may increase erosion dramatically and emphasize the need to preserve forests in this part of the country. Mentioned examples show that RUSLE is a widely recognized method of erosion estimation. Its application reaches beyond the original field of agriculture and spreads over land use management, natural environment protection and other.

3.2.3 Erosion Potential Method - Gavrilovic Method

Erosion Potential Method (EPM), also called Gavrilovic Method after its creator Slobodan Gavrilovic, is the result of study on the Morava river catchment in Serbia in the 1960's. The base of EPM is the Method for the Quantitative Classification of Erosion, which was formally proposed in 1954[19]. Gavrilovic method requires both qualitative and quantitative data as an input and gives three main quantities as an output:

- Total annual volume of detached soil W - which is the amount of soil available to be eroded due to erosion processes and basin characteristics $[m^3/\text{year}]$

- Sediment delivery ratio R - which describes the quantity of the soil that leaves the watershed [-]

- Actual sediment yield G - amount of soil that reaches the tow of the watershed thorough the river system $[m^3/\text{year}]$

The EPM method consists of the following equations:

$$\begin{gathered} G = WR \\ W_s = \pi H \tau_G Z^{3/2} A \\ \tau_G = [(T/10) + 0.1]^{1/2} \\ Z = XY(\xi + S^{1/2}) \\ R = \frac{\sqrt{OD}(l + l_i)}{(l + 10)A} \end{gathered} \tag{3.5}$$

Where:

- τ_g is the temperature coefficient [°C]
- H is the mean annual precipitation [mm/year]
- Z is the erosion coefficient [-]
- A is the area of the basin [km^2]
- O is the perimeter of the basin [km]
- D is the mean altitude of the basin [km]
- l is the length of the main river [km]
- l_i is the total length of the minor rivers [km]
- T is the mean annual temperature of the basin [°C]
- S is the mean slope of the basin [%]
- X is the soil protection coefficient [-]
- Y is the erodibility coefficient [-]
- ξ is the kind and extent of erosion coefficient [-]

The following table can be used as a reference for the values of descriptive parameters [19]:

Soil protection coefficient X	
Mixed and dense forest	0.05-0.2
Low density forest with grove	0.05-0.2
Coniferous forest with little grove, scarce bushes, bush prairie	0.2-0.4
Damaged forest and bushes, pasture	0.4-0.6
Damaged pasture and cultivated land	0.6-0.8
Areas without vegetation cover	0.8-1.0
Soil erodibility coefficient Y	
Hard rock, erosion resistant	0.2-0.6
Rock with moderate erosion resistance	0.6-1
Weak rock, stabilised	1-1.3
Sediments, moraines, clay and other rock with little resistance	1.3-1.8
Fine sediments and soils without erosion resistance	1.8-2
Coefficient of type and extent of erosion ξ	
Little erosion on watershed	0.1-0.2
Erosion in waterways on 20-50% of the catchment area	0.3-0.5
Erosion in rivers, gullies and alluvial deposits, karstic erosion	0.6-0.7
50-80% of catchment area affected by surface erosion and landslides	0.8-0.9
Whole watershed affected by erosion	1

Table 3.1: Gavrilovic descriptive factors reference values

At the beginning, EPM was applied in basins of the Balkan Peninsula, in countries like Serbia, Montenegro, Slovenia, Bosnia. Research showed also successful application in Italy and even countries situated far away from Europe as Iran, Chile [20] or Brazil[17]. Its main purpose was to assess the surface erosion. With the recent development of GIS techniques, also this technology is employed to acquire input data for the EPM. In their research [24], Globevnik et al. proposed GIS manipulation techniques to procure data for the EPM, basing on two basins in Croatia and Slovenia. The difference between such obtained sediment yield and the measured one was 20%, which can be seen as a satisfying result. It shows, that Gavrilovic method in combination with GIS tools have a big potential. Before that GIS era, catchments had to be divided into sub-catchments in which the input parameters could be considered uniform.

Yousefi et al. [61] used EPM with GIS and remote sensing to measure sediment yield in Chamagardalan basin in western Iran. Calculated sediment yield was 22.60 [t/ha/year], which, comparing to to 19.97 [t/ha/year] proved to be a reliable result. This analysis was performed with date acquired from a limited number of hydrological stations, proving that EPM may work well in that conditions. Similar work was performed by da Silva et al. [17] in the Tapacura catchment in Brazil. Also their work showed satisfying accordance between the Gavrilovic method (0.108 [t/ha/year]) and the observed sediment yield (0.169 [t/ha/year]). The validity of this method in South Eastern Europe was also confirmed in many studies. Currently, the Gavrilovic method is still being developed and modified. The biggest stress is put on taking advantage of the data provided by GIS. It can lead to a more precise and more thorough prediction of soil erosion in the future.

3.3 Concpetual models

These models usually represent catchments as a series of internal storages. They define the general mechanisms that govern the interchange of sediment

and water between these storages. Input parameters are usually obtained in a calibration with respect to field measured data. Research show that determining the optimal set of values can be cumbersome. In fact, there might be many sets of optimal parameter values and the more complex model is, the harder it is to determine them [35]. It means that the parameters cannot be completely interpreted as physical quantities. This group of models can be seen as an intermediate step between the empirical and physically based ones. Examples of these models will be described in the following subsections.

3.3.1 Agricultural Non-Point Source Pollution Model - AGNPS

AGNPS is an event-based model designed mainly for the use in agriculture. It is capable of simulating runoff, sediment and nutrient transport. The application is limited to small catchments. AGNPS operates on square cells. User selects the size of cell taking into consideration a trade-off between the accuracy of results and the computational effort. Cells with varying dimensions may be used to highlight crucial points in the study area. Input required by the model is the following [3]:

- precipitation
- soil characteristics
- land use
- upland and channel drainage
- agricultural management
- point sources

Algorithm starts with computation of runoff (basing on curve number method), and peak flow. A triangular hydrograph is created for each cell. Then, utilizing previously described USLE the upland erosion is calculated

for each cell in the basin. Then the total mass is subdivided into five classes based on the particle size: large aggregates, small aggregates, sand, silt and clay. Detached soil is then transported from cell to cell using sediment transport and depositional relations. Also erosion coming from riverbanks, riverbed and other sources is accounted for and added to the total result. Model is also capable of simulating transportation of sourcing of nutrients and pollutants, which is definitely crucial in the farming industry, but lies outside the interest of this thesis.

ANGPS provides the user with a sizeable amount of information as output. Among them, the most important are [3]:

- erosivity
- runoff volume and peak flow at the basin outflow
- area-weighted erosion - upland and channel
- sediment delivery ratio
- total sediment yield with division with respect to particle size

A certain amount of study was dedicated to perform the validation of ANGPS and assess its usefulness. Majority of applications refers to agriculture environment and so are the following examples. Mohammed et al. [37] conducted an analysis in Kori watershed in Ethiopia. In confrontation with the measured values, model showed 0.94, 0.90 and 0.98 correlation coefficients for surface runoff, peak runoff rate and sediment yield. This results clearly indicate the good quality of the model. Also, the results of sensitivity analysis pointed on SCS curve number and USLE C factor as the most result affecting parameters. Similar work was done by Haregeweyn and Yohannes [26], in a different region of Ethiopia. Correlation coefficients in this case were also satisfactory: 0.58, 0.96 and 0.95 for the respective outputs. In a different natural environment - Korea, Cho et al. [15] used ANGPS on two small agricultural watersheds - one to calibrate the model and another to validate it. In this case, correlation between observed and simulated runoff, peak flow and sediment yields were 0.97, 0.80 and 0.77 respectively. All these examples show that ANGPS is capable of accurate recreation of reality.

3.3.2 Simulator for Water Resources in Rural Basins - SWRRB

SWRRB, like previously described ANGPS is a conceptual model developed to simulate transportation of water, sediments, nutrient and pollutants in an agricultular watershed. However the difference is that SWRRB can be applied to large and complex basins. It also operates on continuous time-scale and handles subdivision of a basin to take into account changing parameters [16]. The model simulates surface runoff, return flow, percolation, evapotranspiration, sedimentation and also other processes, which are important for farming. Sediment yield is calculated with MUSLE - a modified form of a well-know USLE empirical equation. In SWRRB, like in ANGPS, surface runoff is computed by SCS curve number method. Input required is similar: weather data and basin and sub-basins characteristics, land use etc.

After a completed simulation, SWRRB returns the information on water movements (surface runoff, subsurface flow, soil water content) and sediment movements (sediment yield and pollutant or nutrient transport) on a temporal scale defined by user - daily, monthly or annually.

Arnold and Williams [5] tested the model on 11 watersheds located throughout United States. All study areas represented different climate environments, from humid continental Ohio (65% crop, 22% pasture and 13% grass) to Arizona with hot and desert surroundings (65% desert shrub, 35% grass). Results showed good accordance to the measured values in terms of sediment yield, for example 3.8 to 3.4 [t/ha/y] in Oklahoma and 1.5 to 1.8 [t/ha/y] in Texas. In conclusion, authors point out that the model is an effective tool in simulating water and sediment yields and is a valuable tool to support decision making by the stakeholders.

3.3.3 Large Scale Catchment Model - LASCAM

The goal standing behind the development of LASCAM was to create a model capable of predicting movements of water, sediments and pollutants in large catchments (more than 10000 km^2) over long time periods. In this model, all processes are modelled on the scale of sub-catchments (1-5 km^2 of area,

however utilization of a much bigger sub-catchments may be justified in some cases) and then aggregated to provide the final response of the catchment at the exit point. The sub-catchments are the basic blocks on which the model operates. The following table presents the needed input and the output data [58]:

Input	Output
Daily distributed rainfall	Surface runoff
Pan evaporation	Subsurface runoff
Land use information	Actual evaporation
Topographic data	Recharge to the permanent groundwater table
Measured stream flows (for calibration)	Baseflow
	Soil moisture

Table 3.2: LASCAM input and output

To predict erosion generation, a conceptualization of the Universal Soil Loss Equation is adapted. Once eroded, sediments are transported in streams and this transport is governed by stream sediment capacity. If sediment quantity is greater than the capacity, it is subjected to deposition on the riverbed and river banks and it is available for erosion in the future. In an opposite situation (stream transport capacity not fulfilled), the erosion is taking place in the stream banks.

Viney and Sivapalan [58] have employed LASCAM model to Avon River basin in Western Australia. It is a large and dry basin that occupies the territory of 119000 km^2. To apply the model, they have split this big zone into 137 sub-catchments with 888 km^2 of mean area. The results of sediment yield they presented allow to state that the prediction is generally in accordance with the observed data. The drawback of the model mentioned is the lack of discrimination into particle sizes.

3.4 Physically based models

The last group of models described will be physically based models. These models are the most complex ones - they try to understand the processes that take place in reality, like the impact of a raindrop onto soil and consequent detachment of soil particle. These models usually rely on the solutions of mass and momentum conservation equations of flow and mass conservation equation for sediments. They require a big amount of input data, which unfortunately often is scarce or inconsistent. This leads to errors in output, which can be seen as a drawback that generally applies to all the models of this group. Another problem is the "overparametrisation" - tens or even hundreds of parameters that these models include make it almost impossible to find the "best-fit" solution [35]. Although the parameters have physical meaning and should be measured in field, it is sometimes impossible in practice due to their temporal and spatial variability. This implies the necessity to calibrate them in confrontation the measured data, what makes them lose their physical meaning. Lastly, the equations that the models rely on were derived for small scale and in specific conditions. There is no guarantee, that they will yield accurate results if applied to a big scale and different environment. Despite the drawbacks that these models have, they present the biggest potential in recreating the erosion phenomenon. A lot of study must be done to develop and optimise a model which is accurate and not over complicated. Some physically based models that are now is use will be presented in the following paragraphs.

3.4.1 Limburg Soil Erosion Model - LISEM

LISEM was developed in the beginning of th 90's by the Dutch scientists from the University of Utrecht. This physically based model was one of the first to be completely incorporated into a GIS raster, which means that there is no conversion needed and the model can be operated in the GIS environment [52]. This brings further advantages - a large amount of data needed to run the model can be obtained straight from GIS instead of typing it by hand. LISEM employs a series of mathematical equations to model

processes that lead to soil erosion. Full description can be found in literature [51]. As an example, soil detachment from raindrop impact is simulated with the following one:

$$DETR = \left[\frac{2.82}{AGGRSTAB} KE \exp\left(-1.48 DEPTH\right) + 2.96\right](P - I)\frac{dx^2}{dt} \tag{3.6}$$

where: DETR - is the splash detachment $[\frac{g}{s}]$
AGGRSTAB - is the soil aggregate stability (median number of drops) [-]
KE - is the rainfall kinetic energy $[\frac{J}{m^2}]$
DEPTH - is the depth of the surface water layer [mm]
P - is the rainfall [mm]
I - is the interception [mm]
dx - is the size of an element [m]
dt - is the time increment [s]

The input needed is the rainfall and rain gauge map, soil water model and a series of maps defining land use, morphology etc. As an output, LISEM produces a map of erosion and deposition of soil. Amongst the advantages of the model, there can be listed: basing on mathematical laws wherever that is possible and limiting the empirical dependencies; all variables can be directly measured in field; easy adaptability for changes; full integration with GIS; user friendly output maps that can be read not only by specialists. The disadvantages, on the other hand, may include a big need for input data (intrinsic characteristic of physically based models) and existence of some empirical relations.

Sensitivity analysis performed by De Roo and Jetten [50] pointed out that the model is the most sensitive to water conductivity, slope gradient and roughness (Manning's coefficient). Application of LISEM in basins in the Netherlands and South Africa, showed that the results, after calibration of the model, may be seen as reliable [51]. The existing difference, according to authors, can be explained by the uncertainty in the measured data.

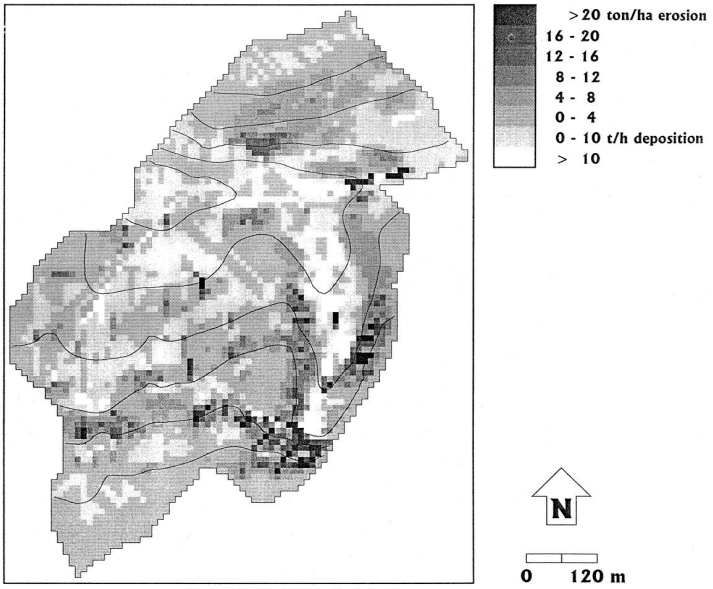

Figure 3.2: An output example of LISEM. Source:[51]

3.4.2 Water Erosion Prediction Project - WEPP

Water Erosion Prediction Project is the effect of work done in US Department of Agriculture. It is a physically-based model for predicting erosion and water movement in small and medium basins. It consists of several components[53]:

- stochastic weather generator that simulates daily climatic data
- infiltration/runoff module based on Green-Ampt infiltration equation
- soil-water balance module based on the one from SWRRB model
- vegetation growth module
- module describing decomposition of plant residues
- irrigation module

The model computes soil loss along a slope and sediment yield at the end of the hillslope[28]. WEPP takes into account both rill and interrill erosion, describing the latter as soil detachment caused by raindrop or sheet flow. Rill

erosion is depicted in the model as a function of flow's ability to erode sediment, sediment transport capacity and the sediment that is already present in the flow. In the rill erosion phenomenon, the model compares the hydraulic shear stress of flow with the critical stress. If it is greater and if sediment transport capacity of the flow is not exceeded, the erosion takes place. If the opposite situation takes place, that is if the sediment load exceeds sediment transport capacity of the flow, a deposition process occurs.

Nature of input data is similar to the models already described. Rainfall data, morphology, soil characteristic and land-use are necessary to conduct a simulation. Equations, of which the model is composed, can be found in the official documentation of WEPP project [28]. The output is also typical, the most important to mention here is the runoff volume, peak runoff rate and sediment yield.

Amongst the research done on the model, some validation examples are worth noting. Soto and Fierros [53] used WEPP to predict the soil loss in the areas that suffered wildfire in northwest Spain. They compared the 4-year experimental plots with WEPP simulation and obtained correlation coefficients of the order of 0.66-0.68. This result was described as "acceptable" although a tendency to underestimate erosion losses was stressed. In completely other environment, in Karso agricultural watershed in eastern India, Pandey et al. [42] performed a validation and a sensitivity analysis. The results were highly satisfactory, as the R^2 correlation coefficient was between 0.81-0.95 for the sediment yield. The authors also pointed out that the critical parameters in the model are hydraulic conductivity and interrill erosivity for sediment yield while runoff results depend mainly on hydraulic conductivity. A validation was also performed in Italy, on a farm southeast of Bologna. Pieri et al. [44] for the study area obtained the result of 0.03 [t/ha/y] from the simulation, while the observation data showed 0.02-0.15 [t/ha/y]. This comparison again tells us that WEPP tends to underestimate sediment yield.

3.4.3 European Soil Erosion Model - EUROSEM

The idea behind EUROSEM was to create a soil erosion model that would use the best European experience and research. During 1986 European Community Workshop in Bruxelles, the objectives for such a model were outlines. According to [38], it must

- assess the risk of erosion
- be applicable to fields and small catchments
- operate on an event basis
- be a useful tool for selectin soil protection measures

The answer to that was EUROSEM - a fully dynamic event-based model that predicts runoff, soil loss and also produces hydrogrpahs and sediment graphs for each event. Thanks to dynamic approach, it provides advantages over steady-flow methods. It takes into consideration both rill and interrill erosion and can be also used to compute hillslope soil erosion. Two fundamental equations governing the model are dynamic mass balance equation for sediments [38]:

$$\frac{\partial(AC)}{\partial t} + \frac{\partial(QC)}{\partial x} - e(x,t) = q_s(x,t) \tag{3.7}$$

And for water:

$$\frac{\partial(A)}{\partial t} + \frac{\partial(Q)}{\partial x} = r(t) - f(t) \tag{3.8}$$

where: C - is the sediment concentration $[m^3/m^3]$
A - is the cross section of the flow $[m^2]$
Q - is the discharge $[m^3/s]$
q_s - is the external input or extraction of sediment per unit length of flow $[m^3/\mathrm{s/cm}]$
e - is the net detachment or rate of erosion of the bed per unit length of flow $[m^3/\mathrm{s/cm}]$
x - is the horizontal distance
t - is time

$r(t)$ - is the rainfall rate minus interception
$f(t)$ - is the local infiltration rate.

The only erosion types that are not simulated by the model is the erosion coming from ephemeral gullies and from saturation overland flow. To simulate other erosion processes, EUROSEM uses relationships obtained from over 500 experimental observations with shallow surface flows [39].

As an example, EUROSEM was validated in the Catsop watershed in The Netherlands. Folly et al. [22] performed calibration, sensitivity analysis and validation. The conclusions drawn were that the model is not sensitive to changes in initial moisture content of the soil and Manning coefficient. The validation study showed that EUROSEM behaved well when analysing short duration storms, unfortunately results coming from longer storms did not fit well in the observed data. EUROSEM is suffering also from the same drawback as other physically-based models - the difficulty of determination of parameters. Accurate calibration is essential, and even when it's done, there is an uncertainty if the parameters chosen are a good representation of the field conditions.

Summarizing, several approaches have been developed in order to simulate soil erosion accurately. Starting from empirical models from the late 1940's, a huge amount of effort was done to arrive to the currently used, computationally sophisticated physically-based models. Yet no totally satisfying model was developed. Every model quoted in this chapter has some drawbacks and limitations. It implicates, that work in this field is not done. This thesis develops and tests a new physically based model, which will be presented in the following chapters.

Chapter 4

The model equations and their discretization

In this chapter, we present the novel mathematical approach proposed in this thesis to the distributed modelling of soil erosion over a mountain catchment. A set of model equations is introduced, along with an efficient and robust numerical discretization approach. The model is an extension of the original proposal in [7]. Its main novel feature consists in the use of the de Saint Venant equations to model surface water flow over the whole domain, without *a priori* identification of drainage zones. This allows to model basins in which strong variations of the surface runoff occur without *ad hoc* hypotheses, as well as to include naturally lakes and other water reservoirs. Coupled to an efficient and robust semi-implicit discretization method [11], the proposed technique yields an effective spatially distributed. A model based on a similar concept, but employing an explicit time discretization of the de Saint Venant equations, was introduced in [1]. The developments in this thesis allows to overcome the stringent stability restrictions that limited the applicability of the approach proposed in [1].

4.1 Model equations

We consider a domain $\Omega = [0, L_x] \times [0, L_y]$ which contains a basin subdomain $\Omega_b \subset \Omega$, defined by geometric considerations, and a drainage subdomain $\Omega_d \subset \Omega_b$, whose extension varies in time and which is only implicitly defined as the portion of Ω_b where the depth of the surface water layer H is above a minimum threshold. For $x \in \Omega_d$, we model the motion of the surface water

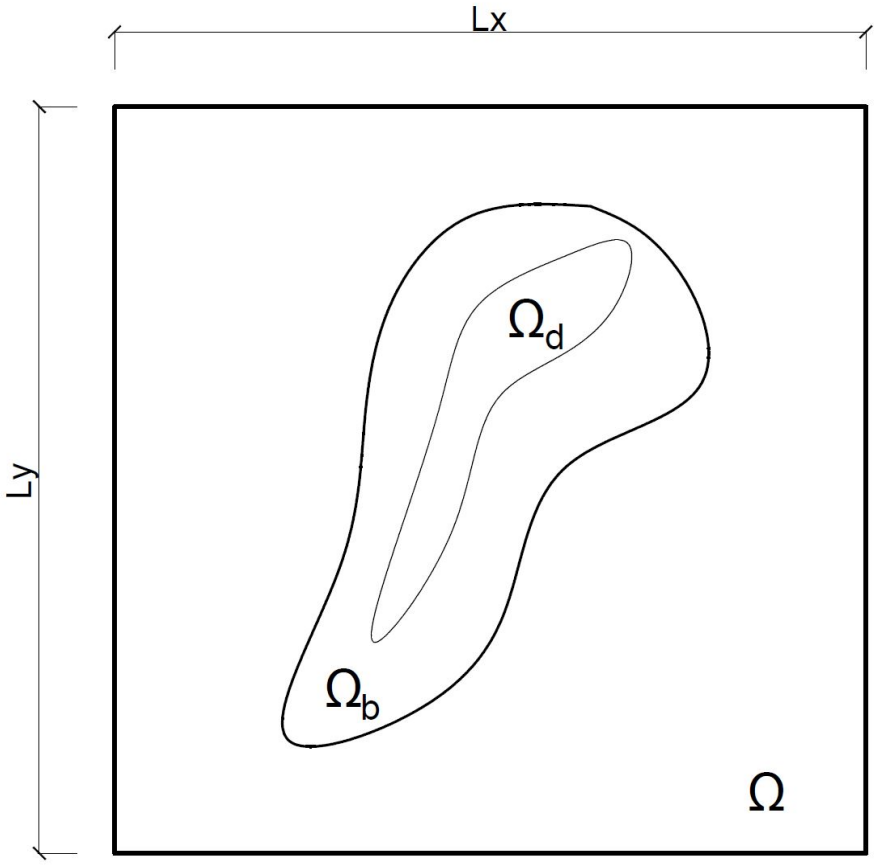

Figure 4.1: Domains' schematics

layer by the de Saint Venant equations

$$\begin{aligned} \frac{\partial H}{\partial t} &= -\nabla \cdot (H\mathbf{u}) + E - I \\ \frac{\partial \mathbf{u}}{\partial t} &= -g\nabla\eta - \mathbf{u} \cdot \nabla\mathbf{u} - \gamma(\mathbf{u})\mathbf{u}. \end{aligned} \tag{4.1}$$

Here b denotes the orographic profile, η is the height of water free surface, so that $H = \eta - b \quad x \in \Omega_d$, $\mathbf{u}$ is the surface water velocity, $\gamma(\mathbf{u})$ is the friction coefficient, E and I are the ground exfiltration and infiltration terms, respectively. They represent the mass exchanges of water between the surface layer and the gravitational layer, to be defined in the following. Notice that we assume that the orographic profile is not changing in time, so that

$$\frac{\partial H}{\partial t} = \frac{\partial \eta}{\partial t}.$$

This simplification is justified in the limit of thin sediment layers. Bed evolution can be taken into account if necessary by a decoupled approach, see [23]. Concerning the friction coefficient, a classical model is given by the Manning formula

$$\gamma(\mathbf{u}) = \frac{gn^2}{H^{4/3}}\mathbf{u}, \tag{4.2}$$

where n denotes the Manning friction coefficient, see e.g. [13]. This coefficient will be computed in this thesis according to the proposal of Rickenmann [49], which is given for each spatial direction by the formula

$$\begin{aligned} \frac{1}{n_x} &= \frac{0.56 g^{0.44} (H|u|)^{0.11}}{S^{0.33} d_{90}^{0.45}} \\ \frac{1}{n_y} &= \frac{0.56 g^{0.44} (H|v|)^{0.11}}{S^{0.33} d_{90}^{0.45}}, \end{aligned} \tag{4.3}$$

where $S = \|\nabla b\|$ denotes the absolute value of the terrain slope and the particle size distribution parameter d_{90} is the maximum grain diameter of 90% of the soil sediment.

The model is then completed by a number of equations for the time evolution of the equivalent depths of other two-dimensional, vertically averaged water and sediment layers, all of which are defined for $x \in \Omega_b$. More specifically, we consider a snow layer with equivalent depth h_n, a sediment layer with equivalent depth h_{sd}, a capillary layer with equivalent depth h_c,

a gravitational layer with equivalent depth h_g and a deep subsurface layer with equivalent depth h_p. For each of these layers, conservation of mass is assumed. For the mass exchanges among layers and for the horizontal mass fluxes, relatively simple models are employed in the present formulation. Each of these could however be replaced by more sophisticated approaches. Notice that, with respect to the models proposed in [7] and [1], no atmospheric layer is explicitly considered and the atmosphere is assumed to be a reservoir of infinite capacity.

The other model equations can be summarised then as

$$\begin{aligned}
\frac{\partial h_{sd}}{\partial t} &= -\nabla \cdot \mathbf{f}_{sd}(H, \mathbf{u}) + W \\
\frac{\partial h_n}{\partial t} &= \mu P - S \\
\frac{\partial h_c}{\partial t} &= C - EV \\
\frac{\partial h_g}{\partial t} &= -\nabla \cdot \mathbf{f}_g(h_g) + (1-\mu)P + S + I - C - D - L \\
\frac{\partial h_p}{\partial t} &= -\nabla \cdot \mathbf{f}_p(h_p) + D.
\end{aligned} \tag{4.4}$$

They will now be discussed in greater detail, starting from the topmost layer and the models employed to compute their source terms are reviewed. The atmospheric component is assumed as a reservoir of infinite capacity, which, as explained before, is not explicitly modelled. Water leaves this reservoir through precipitation (snow or rain), which is characterized by intensity, duration and spatial distribution. On the other hand, water may enter back the atmospheric layer via evapotranspiration.

Precipitation can take the form of rain or snow, depending on the surface temperature. Rain occurs if the temperature is higher then the melting threshold of $T_m = 2\,^{\circ}C$. In this case, water is assumed to infiltrate the soil instantaneously. In the opposite case, precipitation takes the form of snow and is being accumulated at the surface until temperature reaches values high enough to cause melting. The snow layer height in $[m]$ is denoted by h_n. μ is

a nondimensional parameter that takes the value of 1 if temperature is lower or equal than the melting temperature T_m and 0 if it is higher. S is the snow melting rate $[m/s]$, computed according to the Degree-Day approach [43]:

$$S = \delta(T - T_m), \tag{4.5}$$

where δ is a parameter that determines the amount of snow that melts in one day at a given temperature T.

The sediment flux depends on the presence of run-off and on its velocity - $\mathbf{f}_{sd}(H\mathbf{u})$. This correlation is expressed in Grass formula for x and y direction, respectively [18]:

$$\begin{aligned} \mathbf{f}_{SDx} &= a_s u|u|^{b_s} \\ \mathbf{f}_{SDy} &= a_s v|v|^{b_s} \end{aligned} \tag{4.6}$$

Where a_s is a coefficient obtained from experimental data on site that depends on the grain diameter and kinematic viscosity, usually a value between 0 and 1 is taken. The exponent b_s is also empirical and takes value between 0 and 3. In the Grass model, the critical shear stress is set to zero, so the sediment movement begins simultaneously with the water movement.

The source term W, expressed in $[m/s]$, is defined according to the approach proposed by Gavrilovic approach [20] It is the rate of sediment production due to erosive processes as a result of precipitation and it is computed as:

$$W = \pi P \tau_g Z^{3/2} \tag{4.7}$$

Terms τ_g and Z are empirical coefficients of the Gavrilovic method that depend on temperature and land use, respectively, while P is the precipitation intensity in $[mm/s]$. Although the Gavrilovic method gives results on yearly basis, it is assumed that it is also valid for shorter periods in which W will be seen as an intensity.

The capillary layer is the top most zone of the soil, in which capillary forces are able to transmit water toward the surface. Through the process of evapotranspiration, a part of moisture is transmitted to the atmosphere.

Water can also infiltrate to the lower gravitational zone. h_c is the water content in capillary zone expressed in $[m]$, which is limited by the maximum value of water storage capacity [7] $h_{c,max}$ and C is the absorption rate of the capillary zone $[m/s]$

$$C = \max\left[0; k_c\left(\frac{h_g}{h_{g,max}} - \frac{h_c}{h_{c,max}}\right)\right]. \tag{4.8}$$

EV is the evapotranspiration rate expressed in $[m/s]$, computed according to the Thornthwaite approach [2]:

$$PE_m = 1.6\left(\frac{L}{12}\right)\left(\frac{N}{30}\right)\left(\frac{10T_m}{I}\right)^a$$

where T_m is the average temperature for a given month m, L is the monthly mean daytime length, N is the number of days in the month and $I = \sum_{m=1}^{12}\left(\frac{T_m}{5}\right)^{3/2}$ and

$$a = 6.7 \times 10^{-7} I^3 - 7.7 \times 10^{-5} I^2 + 1.8 \times 10^{-2} I + 0.49$$

EV depends on the mean monthly temperatures throughout the year and number of sunny hours in the given month.

The gravitational layer is the soil portion in which water can move due to gravitational forces. This movement is governed mainly by the permeability of the soil and the horizontal fluxes are modelled, as in [7], in terms of the terrain slopes. h_g is the water content in gravitational zone $[m]$, which is limited by the maximum water storage capacity $h_{g,max}$. $\mathbf{f}_g$ are the horizontal fluxes that are formed inside the gravitational zone that govern the movement of water mass $[m^2/s]$. They are defined as:

$$\mathbf{f}_g(h_g) = \beta_g(h_g) h_g \mathbf{n} \tag{4.9}$$

where $\mathbf{n}$ is the unit vector determined by the terrain slope b direction

$$\mathbf{n} = \frac{\nabla b}{\|\nabla b\|} \tag{4.10}$$

and β_g is an empirical coefficient $[m/s]$. L represents hydrological losses $[m/s]$. These losses may occur due to the fact that hydraulic basin does not have to coincide with the hydrogeological basin and thus some water may not arrive to the closing section of the basin. Also, in case of presence of karst aquifers, water may be stored and influence substantially hydrological balance. L is defined as:

$$L = P(1-\phi)(1-\mu), \tag{4.11}$$

where ϕ describes the amount of water that is lost and does not participate in hydrological processes. In the proposed model, hydrological losses are neglected, which implies ϕ equal to 1.

The gravitational layer exchanges mass directly with the surface layer. This process is represented by the ground exfiltration and infilitration terms E and I, respectively. Exfiltration occurs when the maximum water storage capacity in gravitational zone is reached and the excess becomes run-off:

$$\begin{aligned} \text{if} \quad h_g \leq h_{g,max} \quad E &= 0 \\ \text{if} \quad h_g > h_{g,max} \quad E &= \frac{\partial(h_g - h_{g,max})}{\partial t} \end{aligned} \tag{4.12}$$

I is the rate of infiltration of the overland flow in $[m/s]$. When run-off flows over a non-completely saturated soil, that is, where $h_g < h_{g,max}$, water is subjected to infiltration process which is mainly governed by empirical constant k_I expressed in $[s^{-1}]$

$$I = k_I H. \tag{4.13}$$

As already mentioned, the gravitational layer is limited from the top by capillary and from the bottom by deep subsurface layers. The exchange of water by these two layers with the gravitational one is described by the aforementioned capillary absorption rate C and the following value of deep subsurface infiltration D:

$$D = k_p h_g, \tag{4.14}$$

where k_p is an empirical coefficients expressed in $[s^{-1}]$.

The deep subsurface layer is bedrock on which other layers rest. It is more or less fractured, which allows the circulation of water. Movement of water in subsurface (through the fractures) is noticeably slower than the one in the gravitational layer. Also in this case the main factor that describes it is the permeability. h_p is the water content in deep subsurface zone $[m]$. $\mathbf{f}_p$ are are the horizontal fluxes that characterize the movement of water mass in the deep subsurface zone $[m^2/s]$. As in the gravitational case, they are defined as

$$\mathbf{f}_p(h_p) = \beta_p(h_p) h_p \mathbf{n} \tag{4.15}$$

where β_p is an empirical coefficient $[m/s]$.

4.2 Discretization approach

The de Saint Venant equations (4.1) are discretized along the lines of the semi-implicit approach proposed in [11], [12]. A discretization mesh with N_x, N_y constant steps $\Delta x = L_x/N_x$, $\Delta y = L_y/N_y$ in the directions x, y is introduced and with the constant time step Δt. A staggered variable arrangement is employed, with discrete velocity variables $u^n_{i+\frac{1}{2},j}$ and $v^n_{i,j+\frac{1}{2}}$ defined at half integer locations and discrete variables $\eta^n_{i,j}, H^n_{i,j}$ defined at integer locations. The wet cells are defined as those for which $H^n_{i,j} > 0$. These cells provide a discretization of the drainage domain Ω_d. Furthermore, the water layer depths $H^n_{i+\frac{1}{2},j}$, $H^n_{i,j+\frac{1}{2}}$ are defined at the cell edges in an upwind fashion, so that

$$H^n_{i+\frac{1}{2},j} = H^n_{i+1,j} \quad \text{if} \quad u^{n+1}_{i+\frac{1}{2},j} < 0$$

$$H^n_{i+\frac{1}{2},j} = H^n_{i,j} \quad \text{if} \quad u^{n+1}_{i+\frac{1}{2},j} > 0,$$

as suggested in [25]. The cell edges are considered to be wet if the corresponding $H^n_{i\pm\frac{1}{2},j}, H^n_{i,j\pm\frac{1}{2},j}$ water depth values are larger than a minimum

threshold value H_{min}. Otherwise, the edges are assumed to be dry and the corresponding velocity are set to zero. In this way, problems related to the modelling of friction for very thin water layers are avoided, while at the same time water mass conservation is guaranteed.

The space and time discretization is given for all wet cells and corresponding edges by

$$\begin{aligned}
\eta_{i,j}^{n+1} &= \eta_{i,j}^{n} - \frac{\Delta t}{\Delta x}\left[H_{i+\frac{1}{2},j}^{n} u_{i+\frac{1}{2},j}^{n+1} - H_{i-\frac{1}{2},j}^{n} u_{i-\frac{1}{2},j}^{n+1}\right] \\
&- \frac{\Delta t}{\Delta y}\left[H_{i,j+\frac{1}{2}}^{n} v_{i,j+\frac{1}{2}}^{n+1} - H_{i,j-\frac{1}{2}}^{n} v_{i,j-\frac{1}{2}}^{n+1}\right] \\
&+ \Delta t E_{i,j}^{n+1} - \Delta t I_{i,j}^{n+1} \qquad (4.16) \\
u_{i+\frac{1}{2},j}^{n+1} &= \mathcal{F} u_{i+\frac{1}{2},j}^{n} - g\frac{\Delta t}{\Delta x}(\eta_{i+1,j}^{n+1} - \eta_{i,j}^{n+1}) \\
&- \Delta t \gamma_{i+\frac{1}{2},j}^{n} u_{i+\frac{1}{2},j}^{n+1} \qquad (4.17) \\
v_{i,j+\frac{1}{2}}^{n+1} &= \mathcal{F} v_{i,j+\frac{1}{2}}^{n} - g\frac{\Delta t}{\Delta y}(\eta_{i,j+1}^{n+1} - \eta_{i,j}^{n+1}) \\
&- s\Delta t \gamma_{i,j+\frac{1}{2}}^{n} v_{i,i+\frac{1}{2}}^{n+1} \qquad (4.18)
\end{aligned}$$

Here $\mathcal{F} u_{i+\frac{1}{2},j}^{n}$, $\mathcal{F} v_{i,j+\frac{1}{2}}^{n}$ denote some explicit discretization of the momentum advection terms. A simple implementation of the semi-Lagrangian method described in [11] is employed here. While this approach yields a method that is first order only in time and space, the resulting discretization is very robust and stable and allows to employ relatively long time steps in most flow regimes. The practical solution of equations (4.16) is achieved as follows. The equations for $u_{i+\frac{1}{2},j}^{n+1}$, $v_{i,j+\frac{1}{2}}^{n+1}$ are first rewritten as

$$\begin{aligned}
u_{i+\frac{1}{2},j}^{n+1} &= \alpha_{i+\frac{1}{2},j} \mathcal{F} u_{i+\frac{1}{2},j}^{n} - g\alpha_{i+\frac{1}{2},j}\frac{\Delta t}{\Delta x}(\eta_{i+1,j}^{n+1} - \eta_{i,j}^{n+1}) \qquad (4.19) \\
v_{i,j+\frac{1}{2}}^{n+1} &= \alpha_{i,j+\frac{1}{2}} \mathcal{F} v_{i,j+\frac{1}{2}}^{n} - g\alpha_{i,j+\frac{1}{2}}\frac{\Delta t}{\Delta y}(\eta_{i,j+1}^{n+1} - \eta_{i,j}^{n+1}) \qquad (4.20)
\end{aligned}$$

where

$$\alpha_{i+\frac{1}{2},j} = 1/(1 + \Delta t \gamma_{i+\frac{1}{2},j}^{n}), \quad \alpha_{i,j+\frac{1}{2}} = 1/(1 + \Delta t \gamma_{i,j+\frac{1}{2}}^{n}),$$

respectively. These equation are then substituted into the equation for $\eta_{i,j}^{n+1}$, so as to obtain, for the interior nodes, the equations

$$\begin{aligned}
\eta_{i,j}^{n+1} &= \mathcal{G}_{i,j}^{n} \\
&+ g\frac{\Delta t^2}{\Delta x^2}\alpha_{i+\frac{1}{2},j}H_{i+\frac{1}{2},j}^{n}(\eta_{i+1,j}^{n+1}-\eta_{i,j}^{n+1}) \\
&- g\frac{\Delta t^2}{\Delta x^2}\alpha_{i+\frac{1}{2},j}H_{i-\frac{1}{2},j}^{n}(\eta_{i,j}^{n+1}-\eta_{i-1,j}^{n+1}) \\
&+ g\frac{\Delta t^2}{\Delta y^2}\alpha_{i,j+\frac{1}{2}}H_{i,j+\frac{1}{2}}^{n}(\eta_{i,j+1}^{n+1}-\eta_{i,j}^{n+1}) \\
&- g\frac{\Delta t^2}{\Delta y^2}\alpha_{i,j-\frac{1}{2}}H_{i,j-\frac{1}{2}}^{n}(\eta_{i,j}^{n+1}-\eta_{i,j-1}^{n+1})
\end{aligned} \tag{4.21}$$

where

$$\begin{aligned}
\mathcal{G}_{i,j}^{n} &= \eta_{i,j}^{n} + \Delta t E_{i,j}^{n+1} - \Delta t I_{i,j}^{n+1} \\
&- \frac{\Delta t}{\Delta x}\left[H_{i+\frac{1}{2},j}^{n}\alpha_{i+\frac{1}{2},j}\mathcal{F}u_{i+\frac{1}{2},j}^{n} - H_{i-\frac{1}{2},j}^{n}\alpha_{i-\frac{1}{2},j}\mathcal{F}u_{i-\frac{1}{2},j}^{n}\right] \\
&- \frac{\Delta t}{\Delta y}\left[H_{i,j+\frac{1}{2}}^{n}\alpha_{i,j+\frac{1}{2}}\mathcal{F}v_{i,j+\frac{1}{2}}^{n} - H_{i,j-\frac{1}{2}}^{n}\alpha_{i,j-\frac{1}{2}}\mathcal{F}v_{i,j-\frac{1}{2}}^{n}\right].
\end{aligned} \tag{4.22}$$

Equation (4.21) can be rewritten as

$$\begin{aligned}
&\left[1 + g\frac{\Delta t^2}{\Delta x^2}\left(\alpha_{i+\frac{1}{2},j}H_{i+\frac{1}{2},j}^{n} + \alpha_{i-\frac{1}{2},j}H_{i-\frac{1}{2},j}^{n}\right)\right. \\
&\left. + g\frac{\Delta t^2}{\Delta y^2}\left(\alpha_{i,j+\frac{1}{2}}H_{i,j+\frac{1}{2}}^{n} + \alpha_{i,j-\frac{1}{2}}H_{i,j-\frac{1}{2}}^{n}\right)\right]\eta_{i,j}^{n+1} \\
&- g\frac{\Delta t^2}{\Delta x^2}\alpha_{i+\frac{1}{2},j}H_{i+\frac{1}{2},j}^{n}\eta_{i+1,j}^{n+1} - g\frac{\Delta t^2}{\Delta x^2}\alpha_{i-\frac{1}{2},j}H_{i-\frac{1}{2},j}^{n}\eta_{i-1,j}^{n+1} \\
&- g\frac{\Delta t^2}{\Delta y^2}\alpha_{i,j+\frac{1}{2}}H_{i,j+\frac{1}{2}}^{n}\eta_{i,j+1}^{n+1} - g\frac{\Delta t^2}{\Delta y^2}\alpha_{i,j-\frac{1}{2}}H_{i,j-\frac{1}{2}}^{n}\eta_{i,j-1}^{n+1} = \mathcal{G}_{i,j}^{n}.
\end{aligned} \tag{4.23}$$

These equations, defined for all wet cells, indentify a linear system whose matrix is symmetric, positive definite and diagonally dominant, thus guaranteeing the possibility of a fast and accurate numerical solution by the preconditioned conjugate gradient method. All other equations in (4.4) can

be cast in the generic conservation law form with sources

$$\frac{\partial c}{\partial t} = -\nabla \cdot \mathbf{f} + Q.$$

These are all discretized by a finite volume approach over each cell of the computational domain, with first order upwind definitions of the numerical fluxes $f_{i\pm\frac{1}{2},j}$, $f_{i,j\pm\frac{1}{2}}$ and explicit Euler time discretization.

Chapter 5

Preliminary tests of the model

In this chapter, the performance of the described model will be tested. For this purpose a simplified orography will be employed - a plane with constant slope and a paraboloidal surface with four local depressions and one hill. The aim of these test are to control if the model produces reasonable results, spot inconsistencies and calibrate empirical parameters.

5.1 Plane surface

5.1.1 Test 1.1 - Impermeable surface

In the first test a plane surface with constant slope is used. Movement of water is described by solution of de Saint Venant equations in a 2D domain. Also the surface is prescribed to be impermeable. This is obtained by setting values of surface infiltration I_{rg} to zero. The domain is a rectangle of dimensions $L_x = 50km$, $L_y = 50km$. The orography is described by:

$$b(x, y) = 4 + 0.0005x + 0.0005y \tag{5.1}$$

Initial condition is a water layer η in the middle part of the slope described by the function:

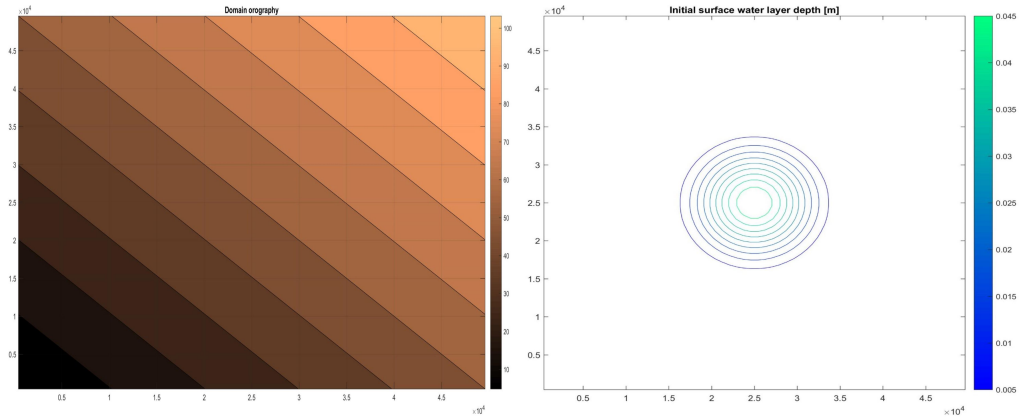

Figure 5.1: Orography (left) and initial condition (right)

$$\begin{aligned} \eta(x,y) &= b(x,y) + 0.05\cos\left(\frac{0.5r\pi}{L_x/4}\right)^3 \\ r &= \sqrt{(x-L_x/2)^2+(y-L_y/2)^2} \end{aligned} \tag{5.2}$$

Summary of parameters is presented in the following table.

Duration	24 h
Number of timesteps	480
L_x	50 km
L_y	50 km
d_x	833 m
d_y	833 m
d_y	833 m
d_{90}	0.1 m

Table 5.1: Test 1.1 parameters

The results are presented in the following picture. They are in accordance with the expectations. Water moves along the biggest slope. This simulation is stable with Courant Number 0.03 and the total CPU time required is 3.44s.

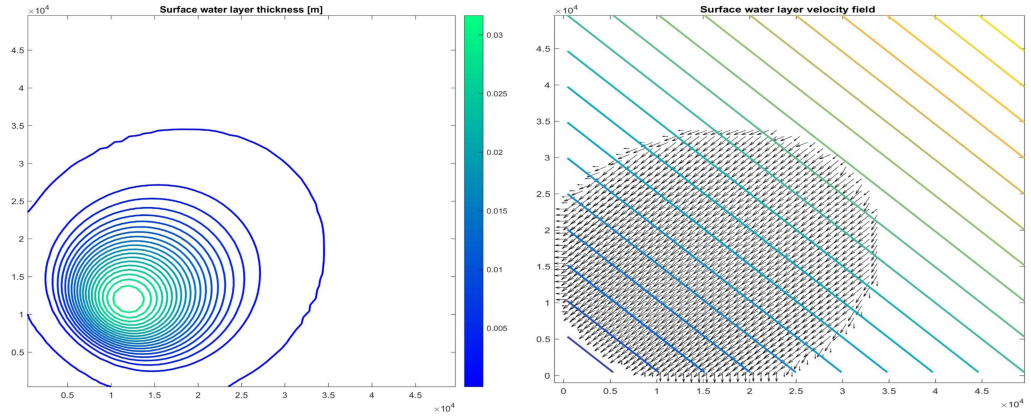

Figure 5.2: Test 1.1 results - final water height (left) and velocity field (right) after time T=24h

5.1.2 Test 1.2 - Movement between layers

The scope of the second test is to observe the movement of water between the capillary, gravitational and deep subsurface layers. Terrain is the same as in the first test. Initial condition is moisture in gravitational layer, which is defined similarly to the initial water surface in Test 1

$$\begin{aligned} h_g((x,y) &= 0.01\cos\left(\frac{0.5r\pi}{L_x/4}\right)^3 \\ r &= \sqrt{(x-L_x/2)^2+(y-L_y/2)^2} \end{aligned}$$

In capillary and deep subsurface zone there is no water at the beginning. Taking into account that both horizontal and lateral transportation of water in soil in a lot slower than its movement on the surface, the simulation time has been extended to 5 days. Values η_g,η_d,C_s,I_{rd}, are in reality very hard to determine as they are function of not only soil type but soil condition as well. Due to this reason, these values were adopted from Bemporad et al. [7]. H_{Gmax},H_{Cmax} were also adapted from [7], choosing "Outcropping rock, outcropping alluvia, present alluvia, areas with active slides" as a pedological class of soil. Evapotranspiration value EV was calculated according to Thronthwhaite, based on meteorological data from the province of Sondrio in Northern Italy.

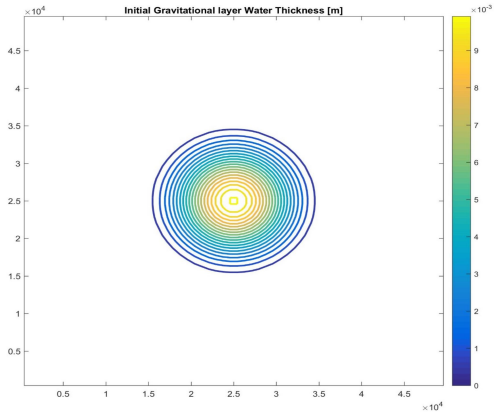

Figure 5.3: Initial condition

Surface friction is described by Manning coefficient, the selected value corresponds to light brush and trees condition. Summary of parameters is presented in the following table.

Duration	120h
Number of timesteps	2400
L_x	50 km
L_y	50 km
d_x	833 m
d_y	833 m
$h_G max$	0.01 m
$h_C max$	0.05 m
η_g	$5 * 10^{-5}$ m/s
η_d	10^{-6} m/s
C_s	$3 * 10^{-5}$ m/s
$I_r d$	10^{-6} m/s
Evapotranspiration	$3.46 * 10^{-8}$ m/s

Table 5.2: Test 1.2 parameters

Results are coherent with expectations. A part of water from the gravitational zone was subjected to capillary action of the upper layer and moved to the upper layer. Another part infiltrated into lower subsurface. Movement

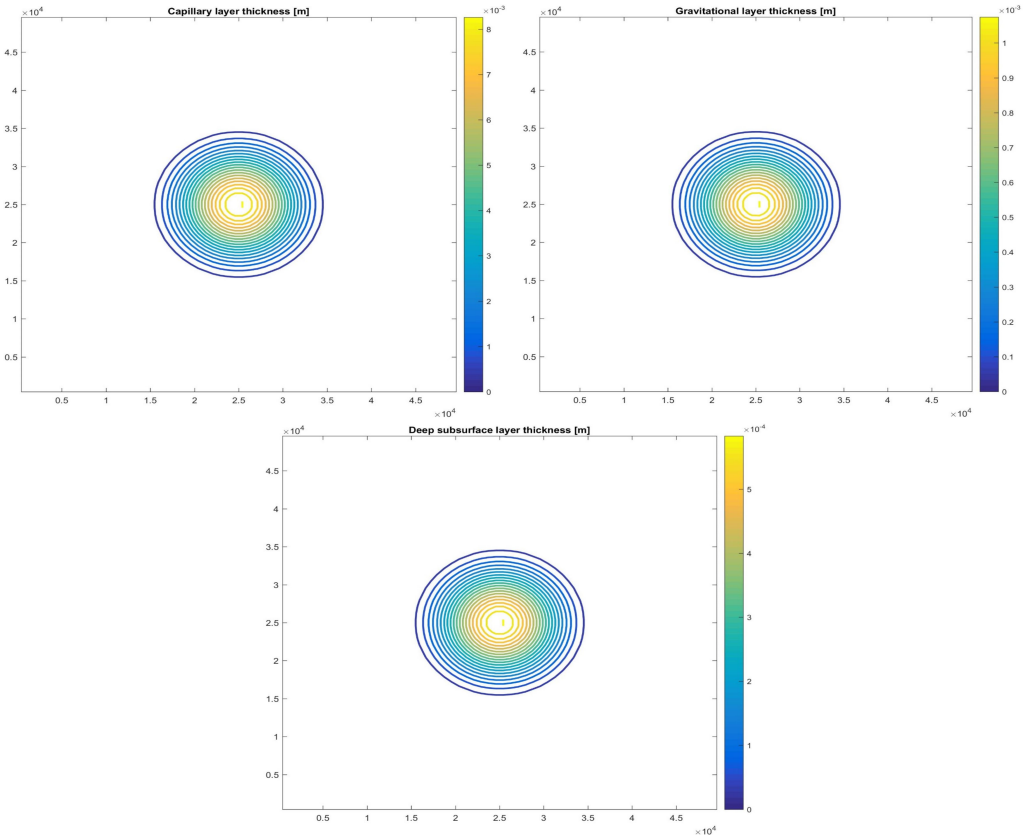

Figure 5.4: Test 1.2 results after time T=120h

of water in horizontal direction is hardly spotted. It is due to the fact that coefficients η_g,η_d governing these movements are relatively low and a longer simulation is needed in order to show these changes. The total CPU time required by the simulation is 18.4s.

5.1.3 Test 1.3 - Run-off infiltration

In the third test both elements are tested together. DSV equations are used to solve the surface run-off while movements in gravitational and deep subsurface layer depend on the gradient of the terrain and proportional terms η_g,η_d. Run-off can now infiltrate into the gravitational layer, provided that it is not yet fully saturated. Hortonian flows, that are surface flows that are formed on the surface of partially saturated soil are not taken into account. Infiltration process is governed by infiltration coefficient I_{rg}. The shape of the initial condition is the same as in the first test - there is a layer of surface water. Parameters of the simulation are summed up in the table.

Duration	120h
Number of timesteps	2400
L_x	50 km
L_y	50 km
d_x	833 m
d_y	833 m
$h_G max$	0.01 m
$h_C max$	0.05 m
η_g	$5 * 10^{-5}$ m/s
η_d	10^{-6} m/s
C_s	$3 * 10^{-5}$ m/s
$I_r d$	10^{-6} m/s
$I_r g$	10^{-5} m/s
Evapotranspiration	$3.46 * 10^{-8}$ m/s

Table 5.3: Test 1.3 parameters

Values show good performance of the model. From the initial surface layer, a major part of water infiltrated into gravitational zone, from which it was

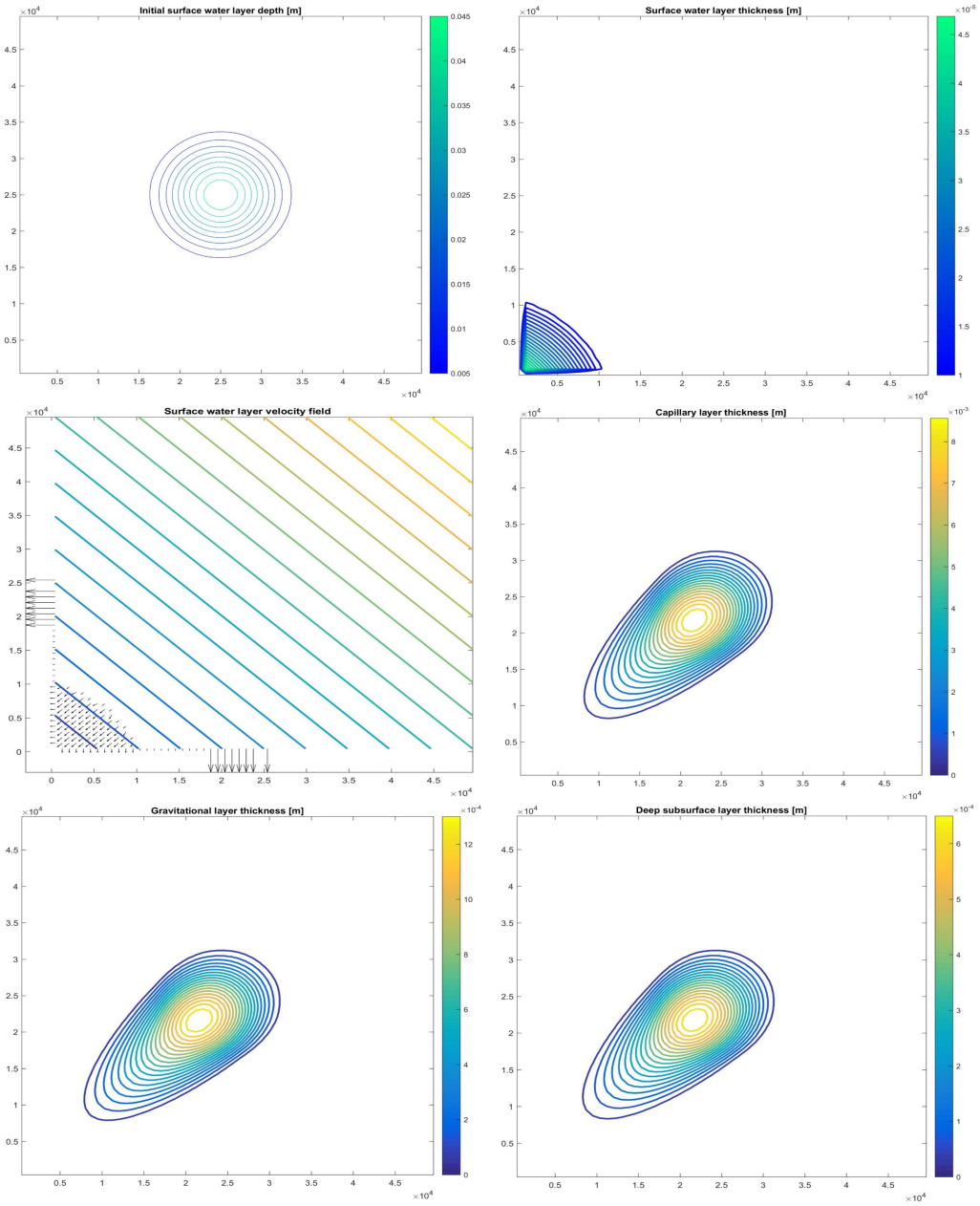

Figure 5.5: Test 1.3 results after time T=120h

partially transported to capillary and deep subsurface zones. There is a correspondence between all the layers. A conclusion can be drawn, that run-off, while moving along the slope, was being absorbed by the soil. Run-off eventually reached the boundary of the domain. The whole simulation is mass conservative with exception of water lost from capillary layer due to evapotranspiration. Simulation took 17.4s and produced stable Courant Number equal to 0.19.

5.1.4 Test 1.4 - Only surface runoff with a fine mesh

In the following test, conditions from 1.1 will be recreated, but with a finer mesh. Domain is now divided into 120x120 mesh, which gives cell size of 416m. To ensure that Courant Number stays below 1, 2 times smaller timestep was taken ($\Delta t = 90\ s$). These changes resulted in CN=0.03. Pictures present the results with comparison to those from Test 1.1.

The general shape of water surface is preserved, however finer mesh produces slightly different results. Boundaries of the water surface are smoother and occupy a little less space. This comes at the computational cost - the 1-day simulation took 11.8 seconds with comparison to 3.44 seconds of the rough-mesh simulation.

5.1.5 Test 1.5 - Fine mesh and a longer simulation

The difference between this test and the previous one is the simulation time. To see the performance in the longer run, duration has been increased to 14 days.

Duration	30 days
Number of timesteps	28800
L_x	50 km
L_y	50 km
d_x	416 m
d_y	416 m

Table 5.4: Test 1.5 parameters

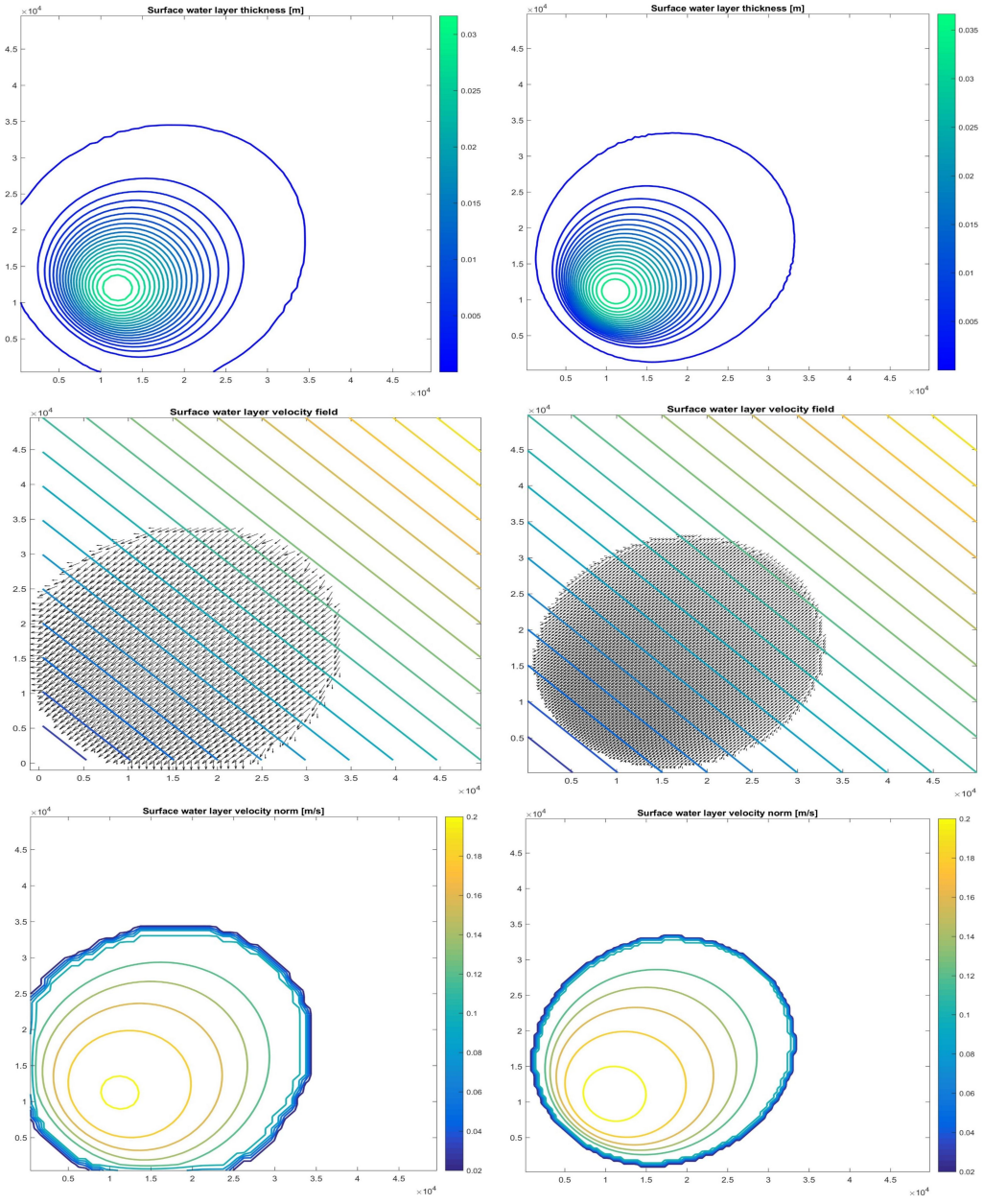

Figure 5.6: Test 1.4 results - rough mesh (left) and fine mesh (right)

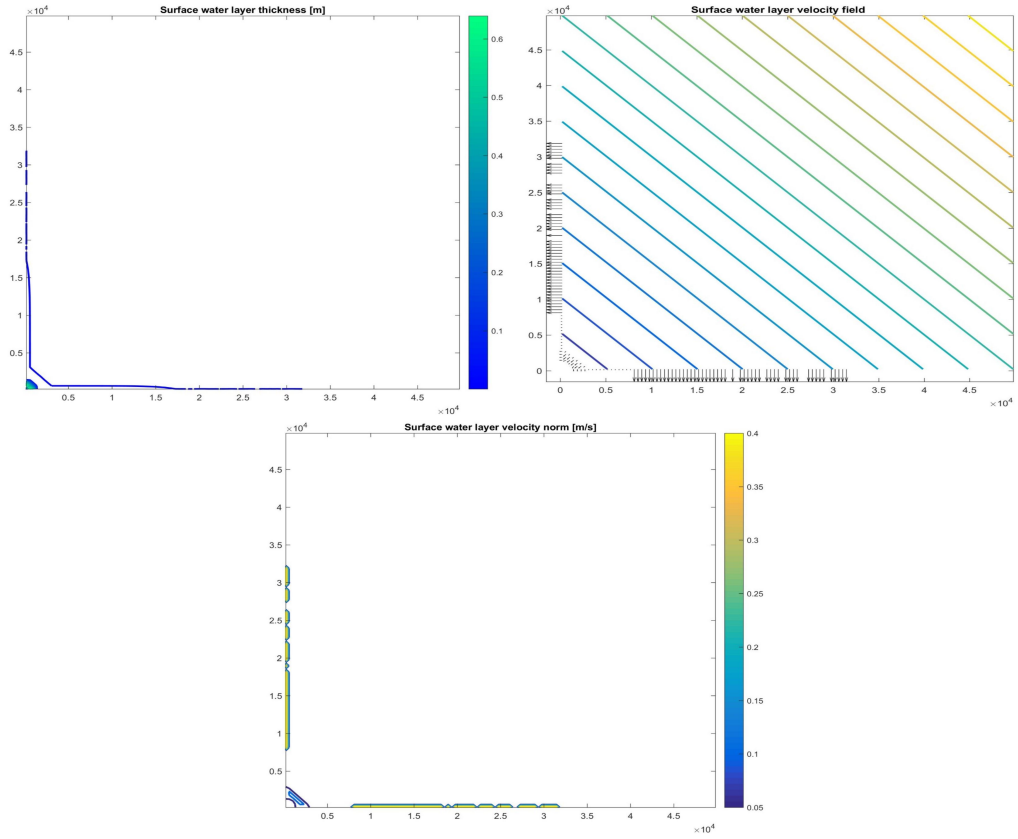

Figure 5.7: Test 1.5 results

The longer simulation produces results that are in accordance with the expectations. Water mass exits the domain through the outflow boundaries. In the longer simulation water would totally exit the domain. If the orography had been shaped differently, i.e. the boundary had not allowed the exit, water would have accumulated at the edge of the domain. Performing this 14-day simulation took 2:59 minutes, which is an acceptable result. Courant Number was stable and equal to 0.381.

5.1.6 Test 1.6 - Runoff infiltration with a fine mesh

Now the impact of mesh refinement will on the whole hydrological model will be assessed. Parameters are the same as in Test 1.3, with the only difference

in the cell size and timestep - both decreased to a half of the original value.

Duration	120h
Number of timesteps	4800
L_x	50 km
L_y	50 km
d_x	416 m
d_y	416 m
$h_G max$	0.01 m
$h_C max$	0.05 m
η_g	$5 * 10^{-5}$ m/s
η_d	10^{-6} m/s
C_s	$3 * 10^{-5}$ m/s
$I_r d$	10^{-6} m/s
$I_r g$	10^{-5} m/s
d_{90}	0.1m
Evapotranspiration	$3.46 * 10^{-8}$ m/s

Table 5.5: Test 1.6 parameters

Finer mesh allows more precise computation of the water movement. The shape of water is a bit different, more irregular with respect to test 1.3. The shape is recreated in the lower layers of the soil. The simulation took 64 seconds compared to the 11.8 seconds on the rough mesh domain. CN=0.381.

5.1.7 Test 1.7 - Runoff infiltration with a fine mesh and a longer simulation time

Fine mesh domain will now be tested with the simulation time of 21 days, which results in 10080 time steps. The rest of parameters form test 1.6 stay unchanged. In a 21-day simulation, water continued to move between layers. Run-off reached the domain boundary, and the shape of water in the undeground layers moved further - the shape is elongated even more. Movement in lower layers is significantly slower than the runoff flow - in 21 days, water mass did not reach the domain boundary. Courant Number was equal to 0.381 and simulation was completed in 7:54 minutes.

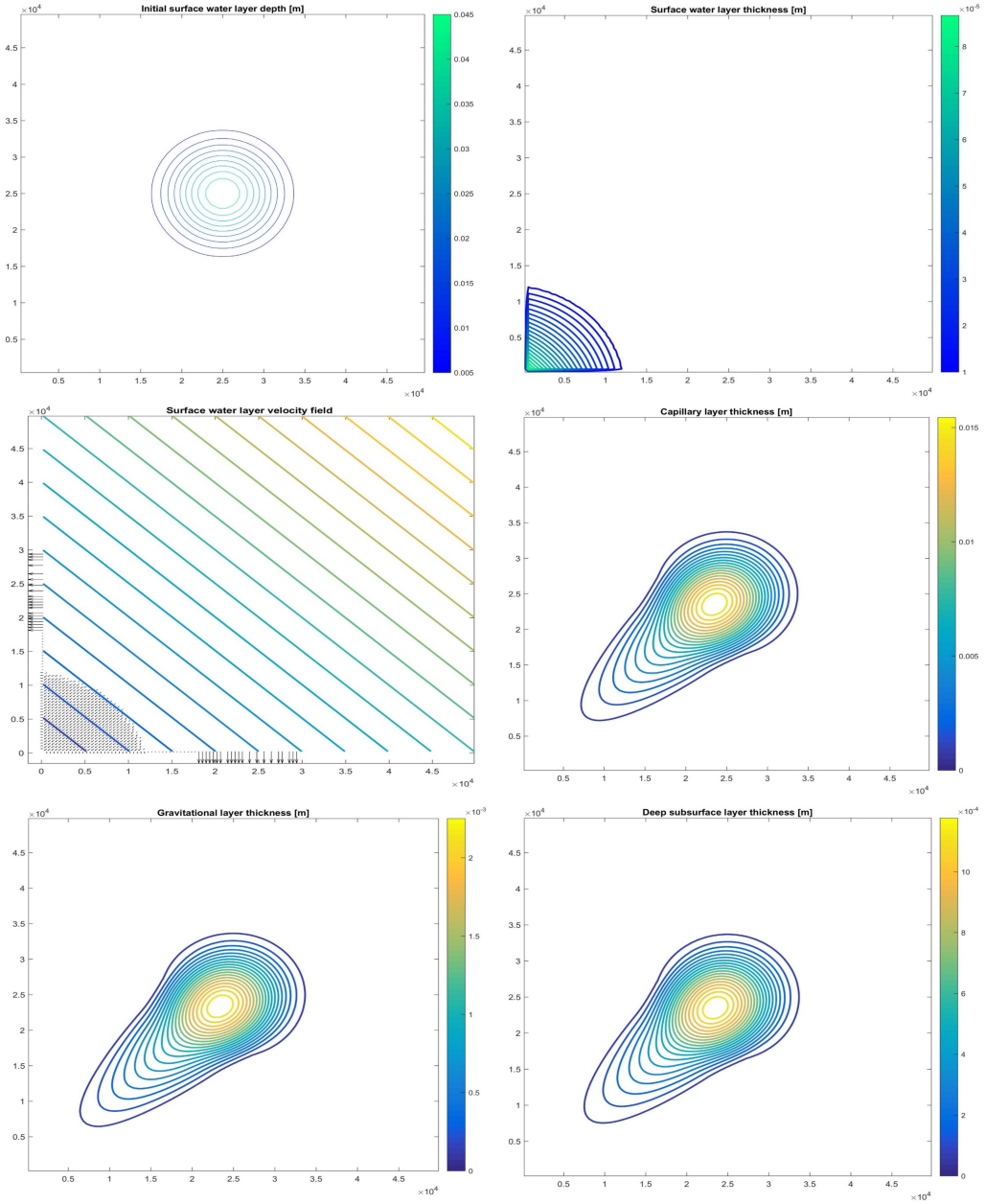

Figure 5.8: Test 1.6 results

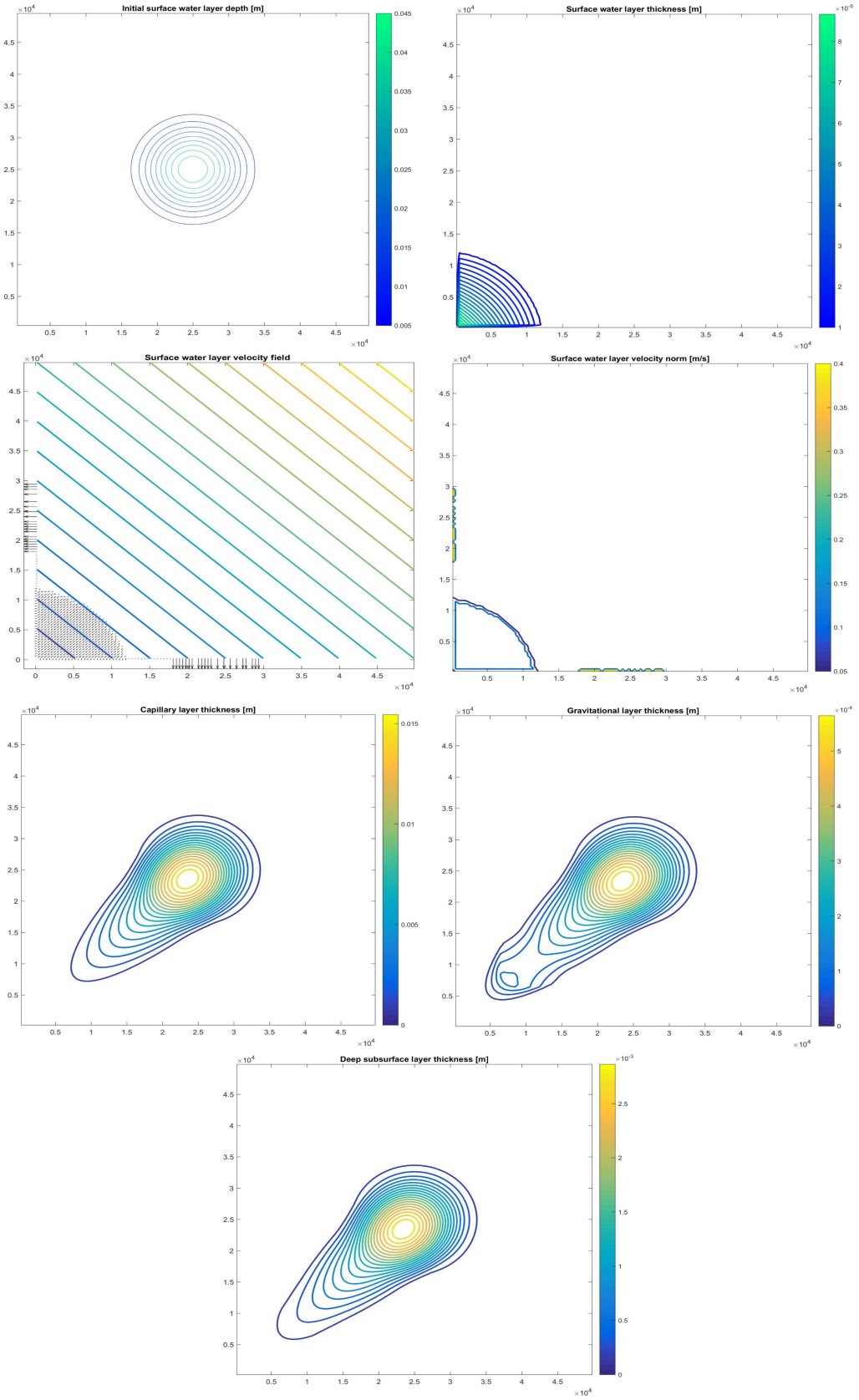

Figure 5.9: Test 1.7 results

5.1.8 Test 1.8 - Sediment transportation

In the following test the ability to model sediment movements will be tested. The initial condition regarding sediments were modelled as a uniform layer of detached soil of 0.1m thickness. Mesh is rough and the simulation time is 1 day. Initial water layer is the same as in the Test 1.1. Terrain surface is set to be impermeable. Sediment movement is connected to water movement.

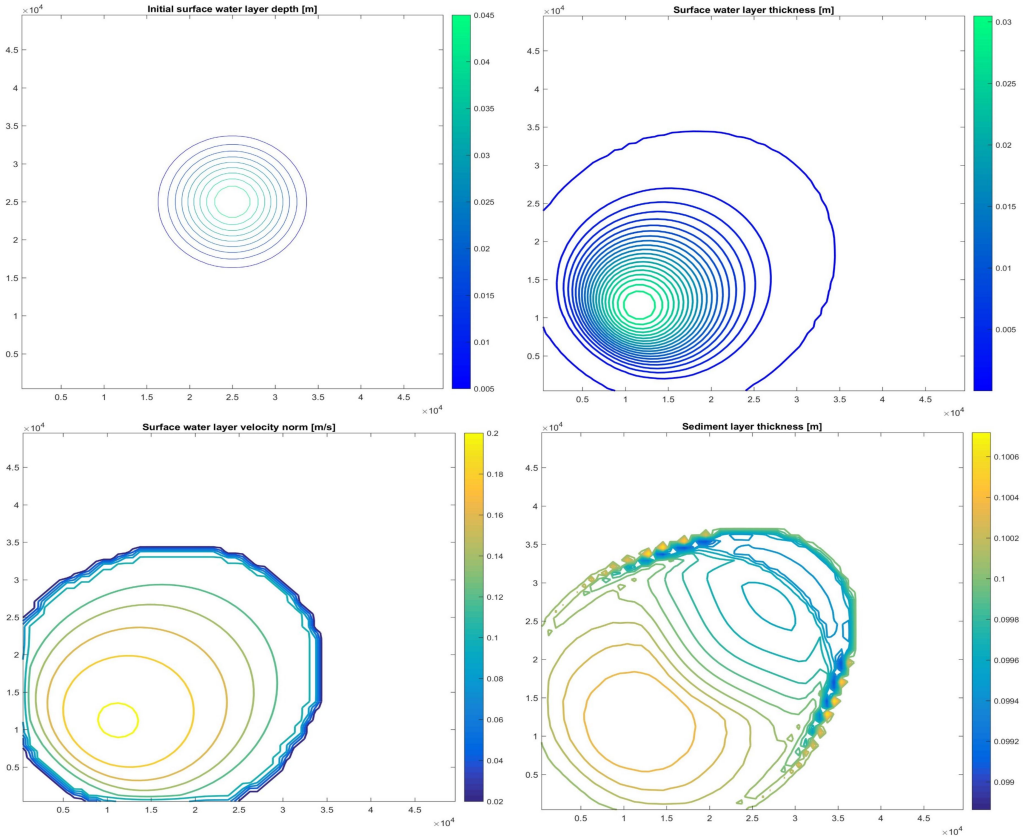

Figure 5.10: Test 1.8 results (T=24h)

This relation is described by Grass formula which depends on water velocity. It can be observed on the graphs - with comparison to the initial 0.1m of sediment, final layer is variable. Sediments are eroded from the area where water was present in the beginning and are deposited in the lower part of the valley. Some deposition can be also seen just above the initial water position - it is the effect of the flattening of the initial water "blob" in the

very first minutes of the simulation. Changes in sediment layer are limited to the area where surface runoff is present - it is consistent with the theory. The differences with respect to initial condition are not big, which shows that in order to move large amount of sediments, a constant supply of flowing water over a long period of time must be provided.

5.2 Paraboloidal surface

In this section, tests will be performed on somewhat more complicated, but still idealized orography. A constant slope terrain will be replaced by a surface consisting of a hill and four valleys. The aim is to see the performance of the model when water depth becomes relatively large and small lakes are created by precipitation. The orography is given by the following equation:

$$b = 15 - 80\frac{(x - 0.5L_x)^2 + (y - L_y)^2}{L_x^2} + 300\frac{(x - 0.5L_x)^4 + (y - L_y)^4}{L_x^4} \quad (5.3)$$

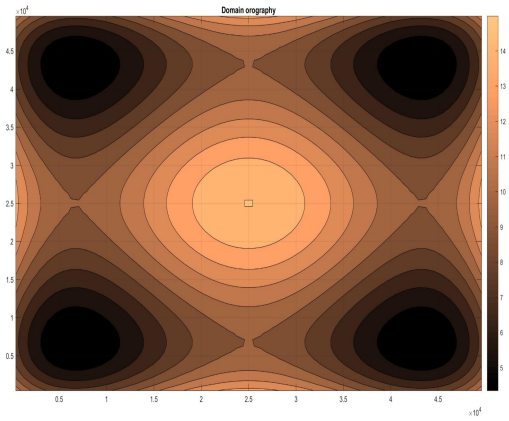

Figure 5.11: Orography in second set of tests

5.2.1 Test 2.1 - Impermeable surface

Analogously to test 1.1, the first test considers an impermeable surface. Time of simulation has been set to 3 days to ensure there is sufficient time to allow

lake formation. The shape of initial condition is the same, however the height of water has been also increased to provide enough water to fill the valleys to a substantial degree. Surface friction is described by Rickenmann formula,

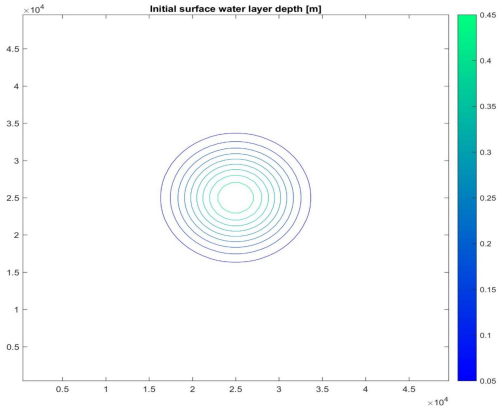

Figure 5.12: Initial condition

which depends on water height and velocity.

Duration	72 h
Number of timesteps	1440
L_x	50 km
L_y	50 km
d_x	833 m
d_y	833 m
d_{90}	0.2 m

Table 5.6: Test 2.1 parameters

The results are presented in the following pictures. Accordingly with the expectations, water moved down the slope and filled valleys up to the value of 0.6m. This shows that de Saint Venant equations are suitable also for modelling a lake formation. Increasing time of simulation, a larger and deeper lake can be observed. Looking at the velocity field diagram, it can be confirmed that water in the valleys is still. Courant number is equal to 0.04 and simulation time is 10.2s.

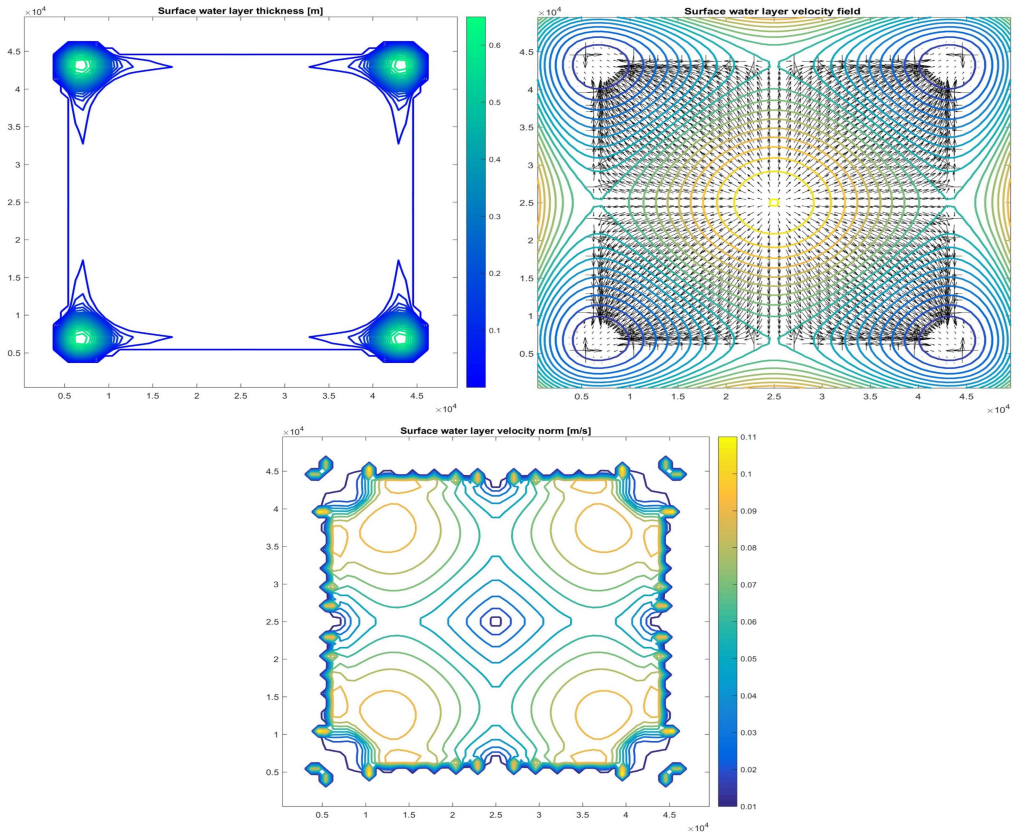

Figure 5.13: Test 2.1 results - after time T=72h

5.2.2 Test 2.2 - Movement between layers

This test is similar to test 1.2. The scope is to observe the movement of water between the capillary, gravitational and deep subsurface layers. Terrain is the same as in the test 2.1. Initial condition is moisture in gravitational layer, which is defined similarly to the initial water surface in Test 2.1. In capillary and deep subsurface zone there is no water at the beginning. Simulation

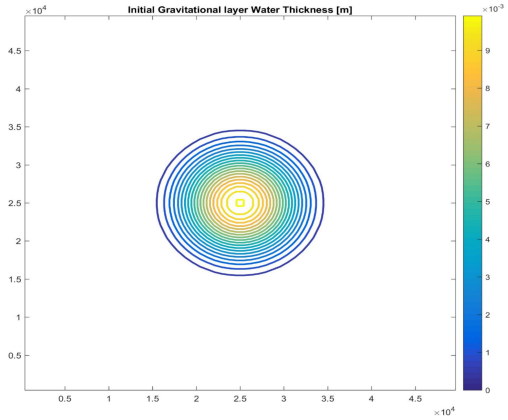

Figure 5.14: Test 2.2 Initial condition

parameters are the same as in the test 1.2.

Duration	72h
Number of timesteps	1440
L_x	50 km
L_y	50 km
d_x	833 m
d_y	833 m
$h_G max$	0.01 m
$h_C max$	0.05 m
η_g	$5 * 10^{-5}$ m/s
η_d	10^{-6} m/s
C_s	$3 * 10^{-5}$ m/s
$I_r d$	10^{-6} m/s
Evapotranspiration	$3.46 * 10^{-8}$ m/s

Table 5.7: Test 1.2 parameters

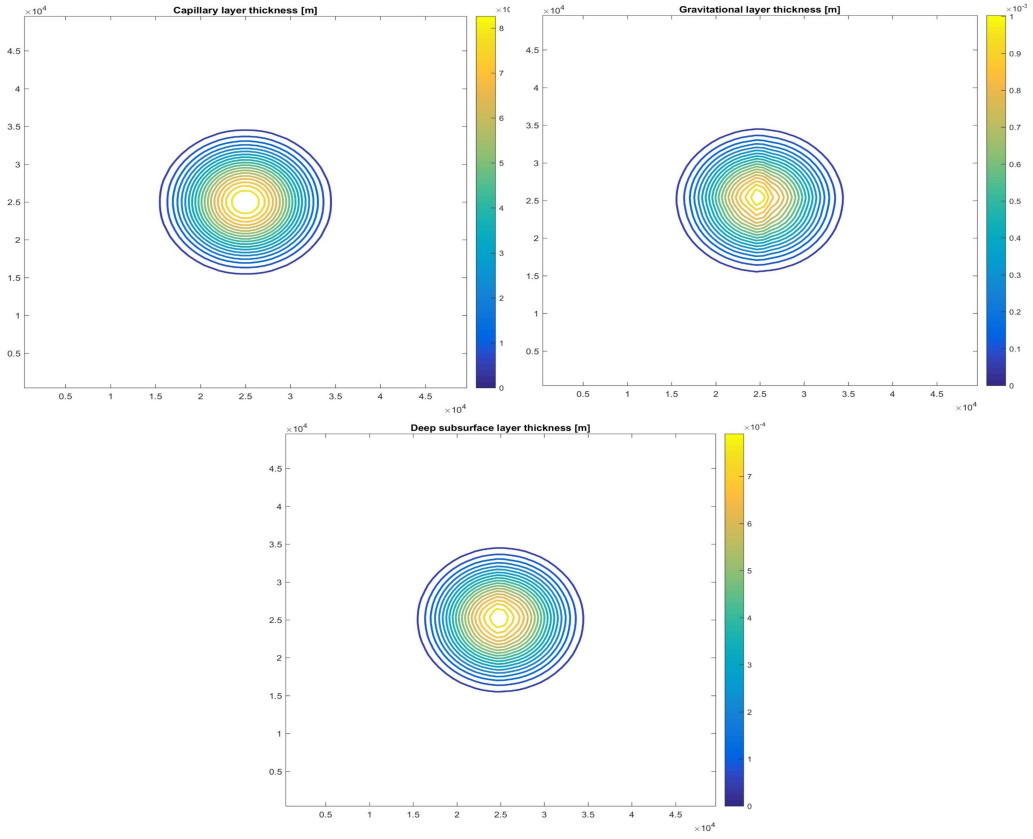

Figure 5.15: Test 2.2 results after time T=72h

Results are the same as in the test with plane surface. Water is transported up and down from the gravitational layer. The spatial extend of water is similar to the one in initial condition which means that the movement of water in deeper zones is not affected by the shape of the terrain which is a conclusion physically reasonable. Time needed to complete the simulation was 16.5s with CN=0.443.

5.2.3 Test 2.3 - Runoff infiltration

In the third test of the second set, both elements will be combined. Parameters of simulation are the same as in 2.2. The height of the initial water layer has been increased in order to present more evident results and avoid whole water being immediately infiltrated into deeper layers. Simulation time is 3

days.

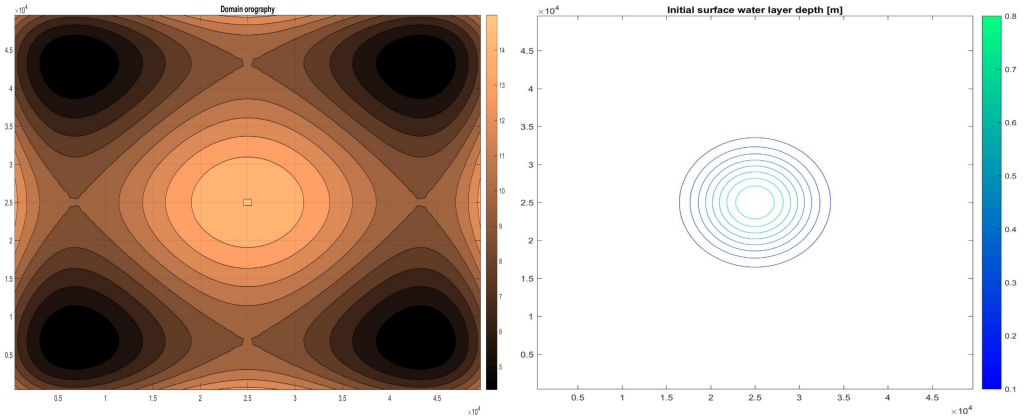

Figure 5.16: Test 2.3 orography and initial condition

Initial water present on the surface was in a major part absorbed by the underlying soil. Capillary layer reached the maximum value h_{cmax} and evapotranspiration process has started. Also in the gravitational zone, the maximum capacity h_{gmax} was reached which provoked exfiltration. Water left on the surface after full saturation of underlying soil follows the maximum gradient of terrain into the valleys. A longer simulation will cause further movement of water from gravitational zone to deep subsurface, which is not limited by any maximum water content. Courant Number in this case was also 0.09 and the simulation took roughly 9.84s.

5.2.4 Test 2.4 - Mesh refinement and sediment transportation

The aim of this test is to check the difference in results when a fine mesh is used. Number of cells in each direction has been doubled giving 120x120 domain which gives 416m cell size. Also time step has been correspondingly halved. Surface is once again impermeable and simulation time is again 3 days. Water height of initial condition has been lowered - maximum value is now 0.45m. the rest of the parameters stay the same as in Test 2.1.

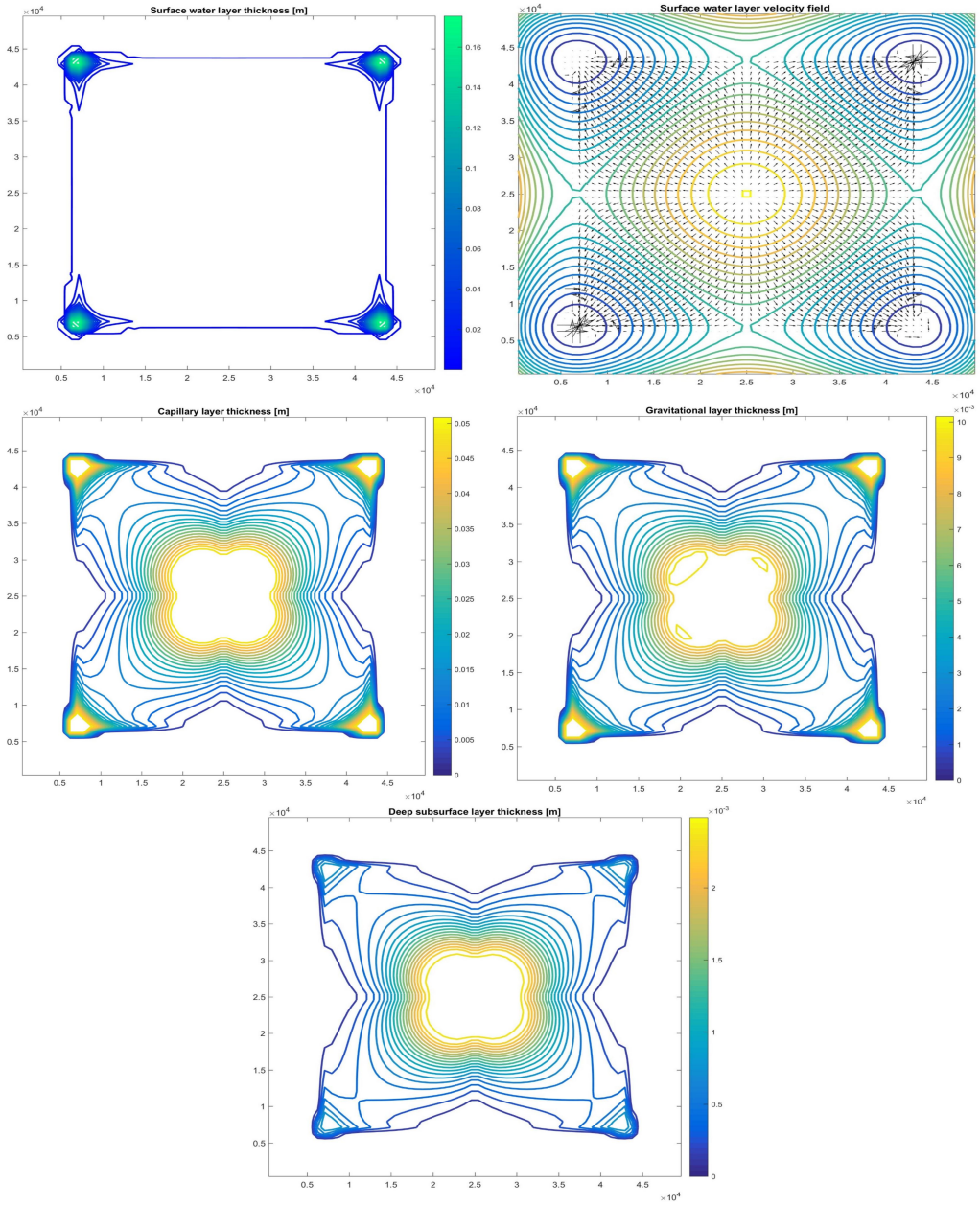

Figure 5.17: Test 2.3 results after time T=72h

Both simulations give similar results in terms of shape. Water is following the maximum slope, fine mesh results can be seen as more precise due to obvious refinement of the domain. Regarding sediment transportation, sediments were transported from the centre of the domain and transported to the

valleys. Variation of water velocity in the closest vicinity of the valleys create adjacent areas of erosion and deposition. This phenomenon can be seen both on rush and fine mesh. Rough mesh: CN=0.04, time of simulation=9.81s. Fine mesh: CN=0.3, time of simulation=36.3s.

5.2.5 Test 2.5 - Rain as initial condition

In all previous tests initial condition was defined as a water mass in a shape of paraboloid that appeared in a certain part of the domain at time t=0. This is of course an unrealistic assumption. In order to employ the model in a realistic case a module that simulates rainfall was introduced into the code. It takes as an input raingauge data, recalculates it and gives as an output the amount of rain water falling on the ground at every timestep. Area of rain can be chosen arbitrarily. In the following test, this area is limited to a rectangle in the central part of the domain. Rainfall intensity is 2mm/h for the whole simulation. Duration of simulation is 3 days.

Looking at the results, it can be stated that the rain module works well. It is raining on the slope of the hill and water, as expected, is flowing down the hill along the biggest slope. Also sediment works well in this case - erosion zone coincide with the rainfall zone, and accumulation can observed at the foot of the hill. The simulation took 9.61 seconds with Courant Number equal to 0.04.

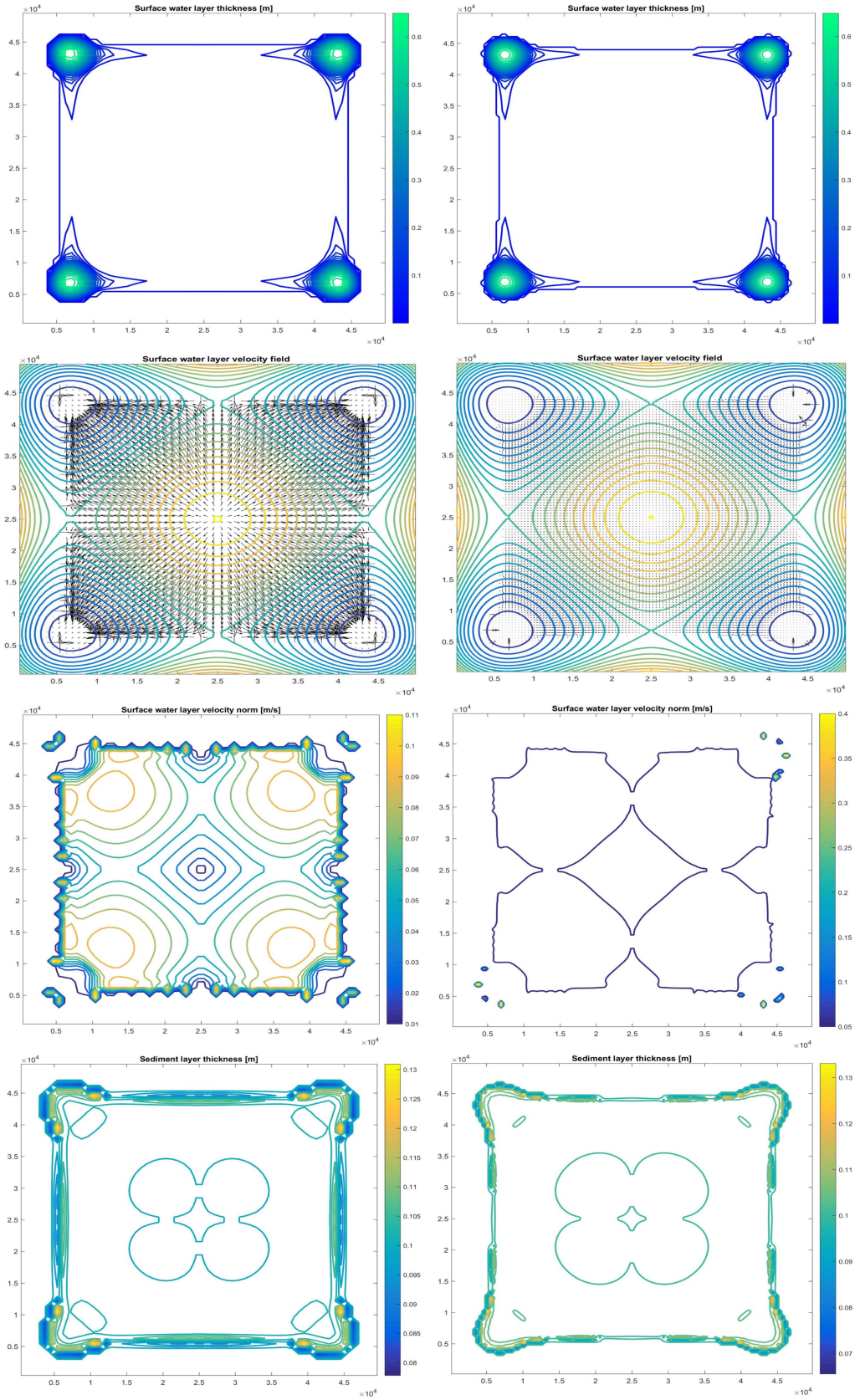

Figure 5.18: Test 2.4 results (left, rough mesh) and fine mesh results (right)

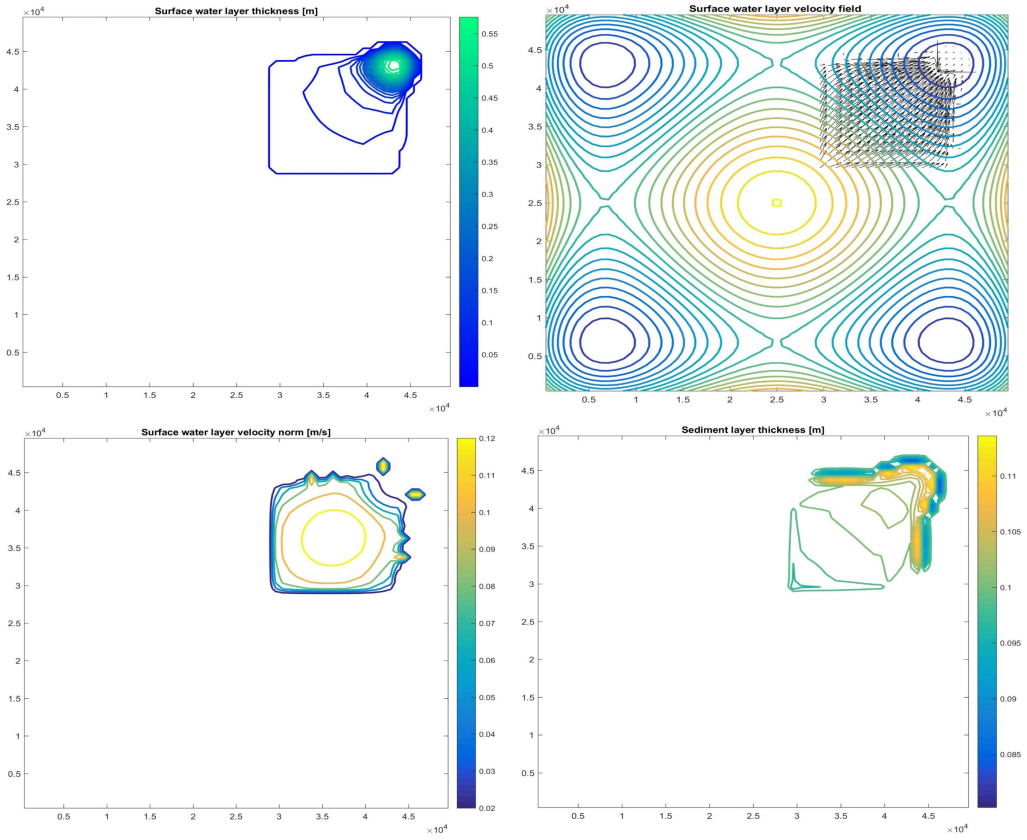

Figure 5.19: Test 2.5 results after T=72h

Chapter 6

Application of the model in a realistic case

Having completed all the tests on idealized orography, the numerical model will now be employed to simulate water and sediment movement on a realistic one. In this way, the usability in common engineering problems can be assessed.

6.1 Area of study

The realistic orography chosen for testing is valley of Tartano, located in Northern Italy in the Province of Sondrio in the Region of Lombardy. Val Tartano is the third largest valley of the lower Valtellina. It is composed of two sub-valleys - Val Lunga (stretching from South-East) and Val Corta (stretching form South-West). The total length is 15km and it is almost entirely situated above 1000m a.s.l.

From morphological point of view, the valley is of glacial origin to which it owes classical "U" shape in the upper part. In the lower part, being subjected to erosive action of water, Val Tartano becomes more "V" shaped. Slopes of the valley are relatively steep, reaching over 35°. From geological point of view, the whole valley is dominated by metamorphic rocks of Morbegno Gneiss which contains a lot of biotite and quartz.

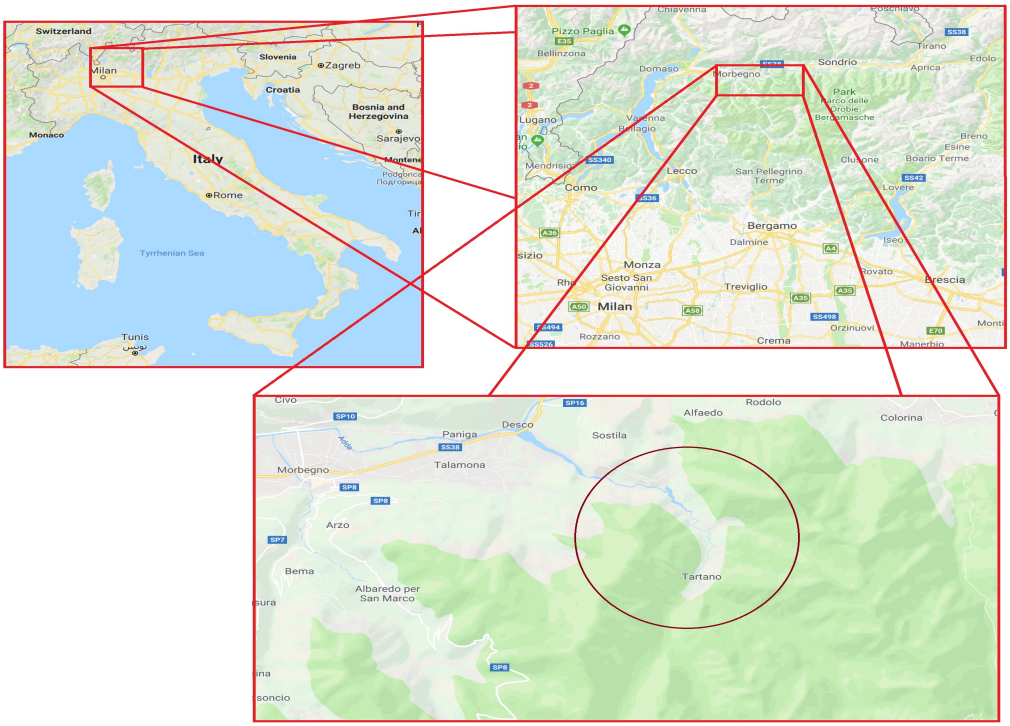

Figure 6.1: Location of Tartano

The main watercourse of the valley is also called Tartano. It is formed by

Figure 6.2: A view of Val Lunga

two streams, one flowing from Val Lunga and one from Val Corta. The one

in Val Lunga takes it source from four small natural lakes situated at 1990m, 2030m, 2095m and 2250m a.s.l. The stream flowing in Val Corta, on the other hand, is constituted by two other streams coming from east (Lemma) and west (Biorca). Val Lunga and Val Corta join at a village of Biorca. From there, Tartano flows as a single stream along the valley and it comes across one dam "di Campo" which was built for hydroelectric purposes. After the dam it forms a broad fan before and flows into river Adda. Summarizing all the tributaries, the total length of the main watercourse is 14.456km [9].

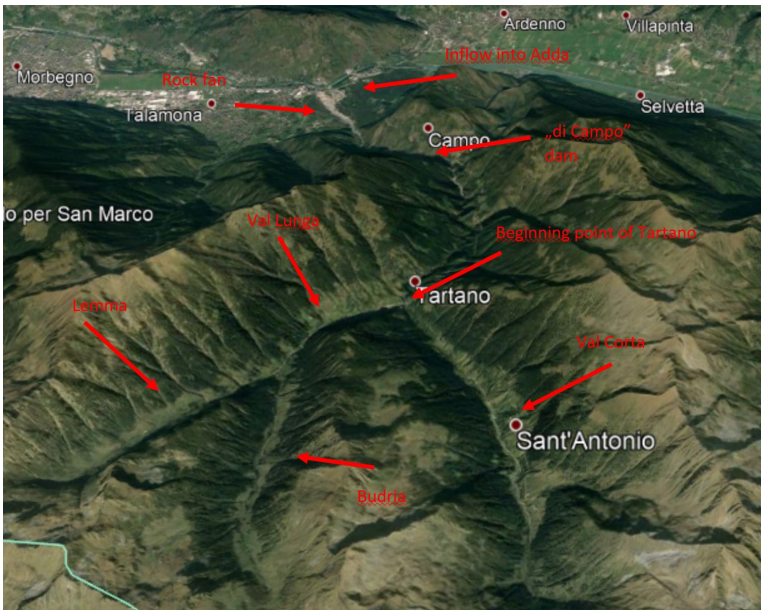

Figure 6.3: Look at Val Tartano

Val Tartano is subject to a high level of hydrogeological risk. As a consequence of some natural phenomena, human life and property may be lost. These phenomena are mainly:

- landslides caused either by soil erosion or human activity,
- mountain floods caused by itense rainfall, snow melt or dam break,
- avalanches in winter

- debris flows, containing both soil and water, travelling at high speed with a big destruction potential,

All of these problems are typical for mountain valleys as they are connected to the presence of steep slopes which facilitate formation of soil mass movement in case of loss of stability and cohesion. For this reason, Val Tartano is a suitable case to test erosion models.

6.1.1 Test 3.1 and 3.2 - Uniform rain on the whole domain with rough and fine mesh

The following simulations will be performed using realistic orography of Val Tartano. Two resolutions will be used - 40x40m, which will be called "fine" and 60x60m, which will be called "rough'. Friction will be computed using Rickenmann formula with the characteristic grain size d_{90} equal to 20cm.

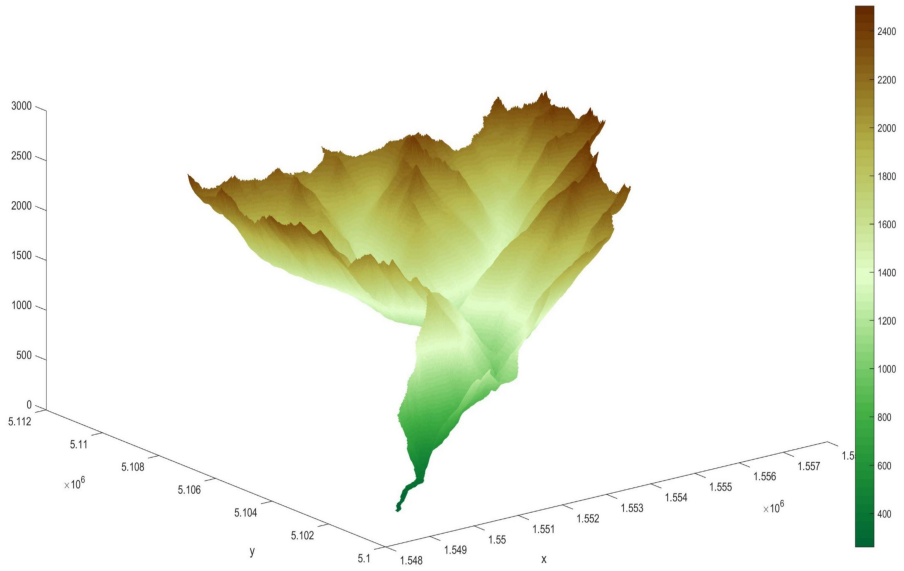

Figure 6.4: Morphology of the valley

Initial condition for this test is a constant 0.01m of equivalent water height in all the 3 layers - capillary, gravitational and deep subsurface. No initial surface water is present, instead a uniform rainfall of 2mm/h is programmed

to last for the first 10 days of the simulation. To avoid initial numerical problems, rain value at time T=0 is set to 0 and then it is interpolated linearly to projected 2mm/h. The total time of simulation is 30 days. Summary of parameters is presented in the table.

Duration of simulation	30 days
Duration of rainfall	10 days
Number of timesteps	14400
Initial condition h_c=h_g=h_d	0.01m
DEM resolution	40x40m (Test 3.1), 60x60m (Test 3.2)
h_{Gmax}	0.01 m
h_{Cmax}	0.05 m
η_g	$5 * 10^{-5}$ m/s
η_d	10^{-6} m/s
C_s	$3 * 10^{-5}$ m/s
I_{rd}	10^{-6} m/s
I_{rg}	10^{-4} m/s
Evapotranspiration	$3.46 * 10^{-8}$ m/s
d_{90}	0.2 m

Table 6.1: Simulation parameters

Looking at the results, similar conclusions can be drawn from both simulations. At time T=30 days, no water was present on the surface. The whole run-off was absorbed by the underground layers which can be seen as reasonable result. In these layers, water moved along the lines of the highest slope, both along the main valley and the tributary ones. Most evident difference can be spotted at the sediment transportation graphs. The fine mesh one is more precise, areas of erosion can be spotted along the main valley. These areas are less evident in the rough mesh. In both simulation, presence of erosion zones prove that at some point run-off was present, which caused the transportation of sediments. Simulation time for rough mesh was 5:23 min and 11:63 min for the fine one. In this case it can be observed that due to more evident sediment transportation results, it is meaningful to dedicate more time and perform the analysis on the fine mesh.

6.1.2 Test 3.3 and 3.4 - Uniform rain over the whole domain with changes in friction parameters

The following simulations will be performed in order to assess the impact of d_{90} parameter on the results. This value, which describes the characteristic grain size for which 90% is finer by weight, is the key component governing the whole friction term according to Rickenmann. To avoid results present in tests 3.1 and 3.2 (the absorption of the whole run-off), simulation time will now be reduced to 10 days and rainfall will be intensified to 5 mm/h. Mesh is "rough" - 60x60m. In Test 3.3 d_{90} will be set to 20cm and in Test 3.4 it will be 5cm. The summary of parameters is in the table.

Duration of simulation	10 days
Duration of rainfall	10 days
Number of timesteps	4800
Initial condition h_c=h_g=h_d	0.01 m
DEM resolution	60x60m
h_{Gmax}	0.01 m
h_{Cmax}	0.05 m
η_g	$5 * 10^{-5}$ m/s
η_d	10^{-6} m/s
C_s	$3 * 10^{-5}$ m/s
I_{rd}	10^{-6} m/s
I_{rg}	10^{-4} m/s
Evapotranspiration	$3.46 * 10^{-8}$ m/s
d_{90}	0.2 m (Test 3.3), 0.05 m (Test 3.4)

Table 6.2: Simulation parameters

In both tests, exfiltration is present after 10 days. The presence of run-off is reasonable, it appears along the line of the highest slope in the main valley of Val Tartano. The height, however remains questionable with local peaks of water height reaching values, which seem to be exaggerated. It can be

seen that $d90$ affects the behaviour of the run-off. In performed simulations, higher value of d_{90} produced exfiltration in more places than the lower one. It must be noted, however, that the final shape and height of surface water depends not only on the friction coefficient but also on the saturation level of the underlying soil. Nevertheless, the difference in the d_{90} provokes different outcomes of simulations.

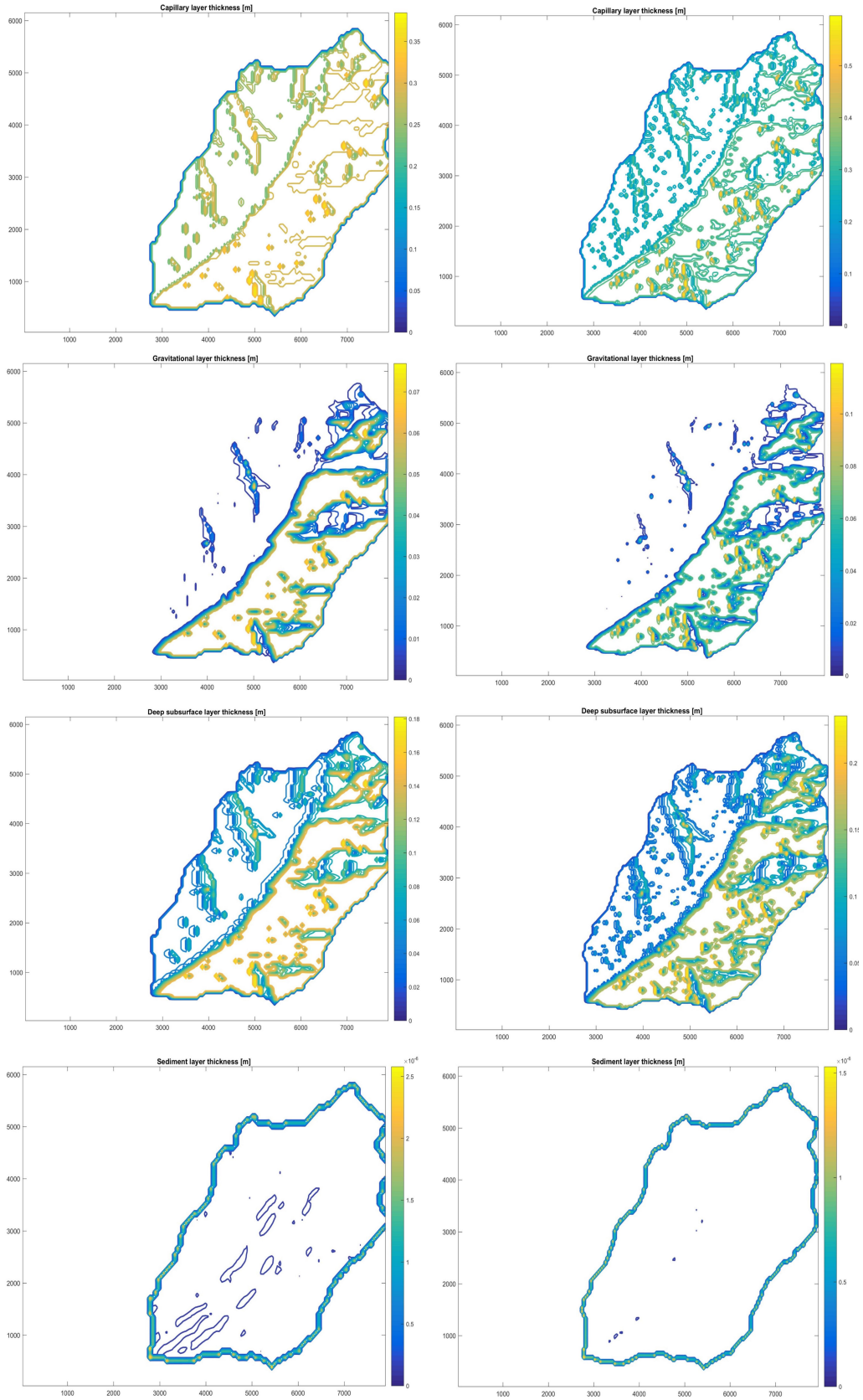

Figure 6.5: Test 3.1 and 3.2 results after T=30 days. 40x40m mesh (left) and 60x60m mesh (right).

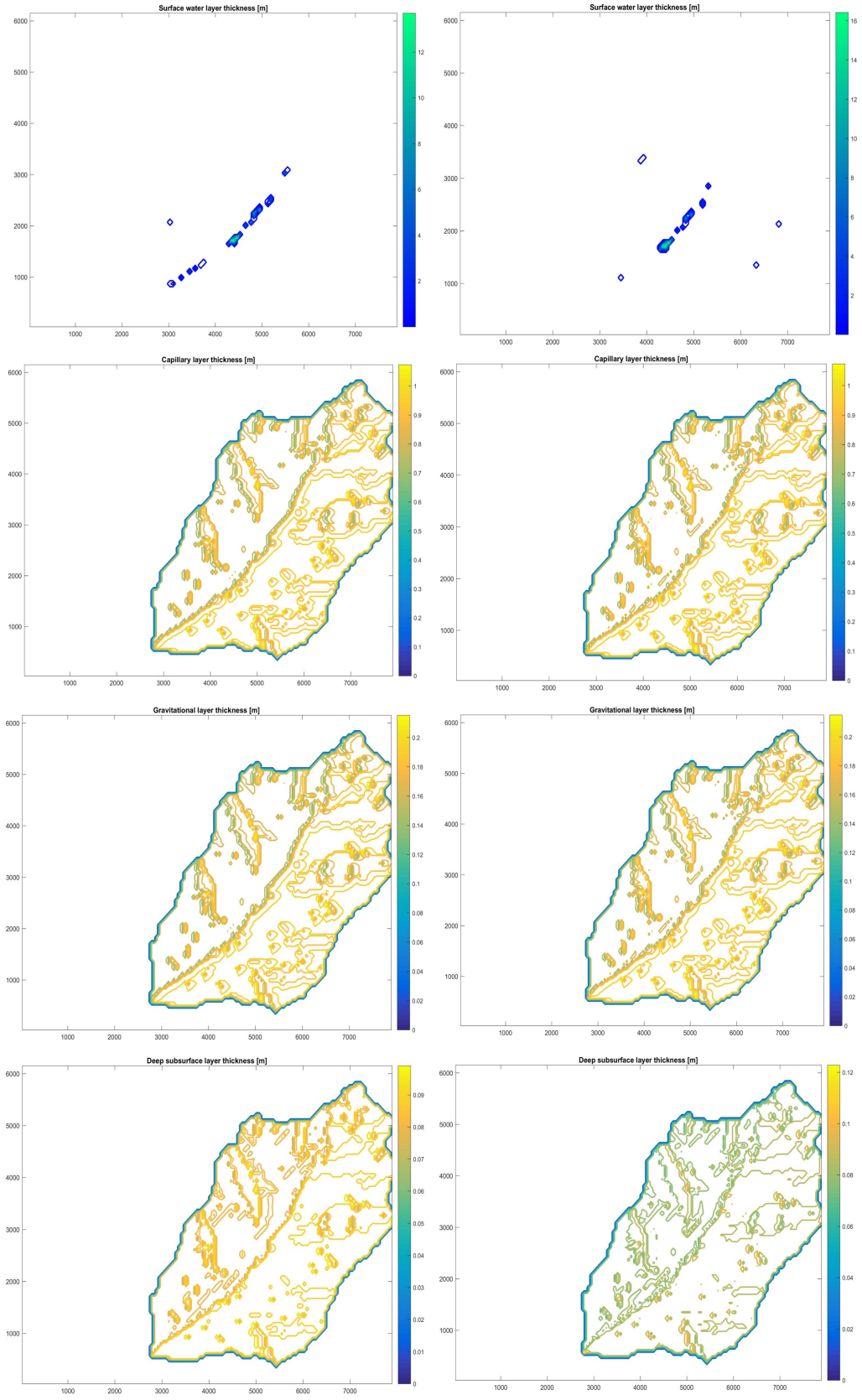

Figure 6.6: Test 3.3 and 3.4 results after T=10 days. $d_{90} = 0.2m$ *(left) and* $d_{90} = 0.05m$ *(right).*

Chapter 7

Conclusion

Performing all the simulations it can be stated that the numerical model presented is promising and on the right way of development. The full 2D implementation of De Saint Venant equations is a noticeable improvement in comparison with the currently used numerical erosion models. The model is also efficient numerically, simulations on idealized surfaces took no more than 20 seconds for 5 days of simulation time.

Regarding the idealized orography, run-off behaved as expected, following the highest slope until the boundary of the domain. Lakes were formed in the valleys in accordance with the expectations. Also movement of water between the underground layers and inside them were physically most probable. Possible fields of further improvement may include introduction of different friction formula than the proposed Rickenmann approach. Friction, alongside with orography, is the main factors governing the water movement. This is why it is worthwhile to propose variety of friction formulation to users, who can then choose the one that performs the best in the given area od study. Also a more sophisticated sediment transportation model can be introduced. The current Grass formula, although producing reasonable results have limitations - it does not take into consideration the availability of sediment to transport. An idea for development may be the implementation of Mayer-Peter-Mueller formula or other similar formulae.

The performance in the model regarding the real case scenario can be described as satisfactory at this stage of work. The movement of both water and sediments follow the implemented laws of physics. In future, more validation should be done in order to spot possible inconsistencies and assess the applicability of the model in areas substantially different than the presented alpine valley of Val Tartano.

ACKNOWLEDGEMENTS

Firstly, I would like to express my gratitude to my supervisors, prof. Luca Bonaventura, prof. Laura Longoni and prof. Davide Brambilla. Without their contribution to the numerical implementation of the model, precious suggestions and insights, the completion of this thesis would certainly not be possible.

Bibliography

[1] A. Abbate. Un modello numerico conservativo di erosione di versante. Tesi di laurea in ingegneria ambientale, Politecnico di Milano, 2015.

[2] F. Acs, H. Breuer, and G. Szasz. Estimation of actual evapotranspiration and soil water content in the growing season. *Agrokemia es talajtan*, 60:57–74, 2011.

[3] L. Ahuja, J. Leppert, K. Rojas, and E. Seely. *Workshop on somputer applications in water management*. Great Plains Agricultural Council, Colorado State University, Fort Collins, CO, 1995.

[4] S.D. Anigma, D.E. Stott, M.K. O'Neil, C.K. Ong, and G.A. Weesies. Soil erosion prediction using rusle for central kenyan highland conditions. *Agricuture Ecosystems & Environment*, 97:295–308, 2003.

[5] J.G. Arnold and J.R. Williams. Validation of swrrb - simulator for water resources in rural basins. *Journal of Water Resources Planning and Management*, 113:243–256, 1987.

[6] Karl Auerswald, Peter Fiener, Walter Martin, and Dirk Elhaus. Use and misuse of the k factor equation in soil erosion medling: An alternative equation for determining usle nomogrpah soil erodibility values. *Catena*, 118:220–225, 2014.

[7] Giorgio A. Bemporad, Julio Alterach, Flavio F. Amighetti, Maximo Peviani, and Italo Saccardo. A distributed apporach for sediment yield evaluation in alpine regions. *Journal of Hydrology*, 197:370–392, 1997.

[8] J.M. Bodoque, A. Diez-Herrero, J.F. Martin-Duque, J.M. Rubiales, A. Godfrey, J. Pedraza, R.M. Carrasco, and M.A. Sanz. Sheet erosion rates determined by using dendromorphological analyis of exposed tree roots: Two examples from central spain. *Catena*, 64:81–102, 2005.

[9] F. Bonacina. Valutazione della produzione di sedimenti di un bacino alpino: stima volumetrica e granulometrica. Tesi di laurea in ingegneria ambientale, Politecnico di Milano, 2010.

[10] John F. Boyle, Andy J. Plater, Claire Mayers, Simon D. Turner, Rob W.Stroud, and Jerry E. Weber. Land use, soil erosion, and sediment yield at pinto lake california: comparsion of a smiplified usle model with the lake sediment record. 2011.

[11] V. Casulli. Semi-implicit finite difference methods for the two-dimensional shallow water equations. *Journal of Computational Physics*, 86:56–74, 1990.

[12] V. Casulli and R. T. Cheng. Semi-implicit finite difference methods for three-dimensional shallow water flow. *International Journal of Numerical Methods in Fluids*, 15(6):629–648, 1992.

[13] H. Chanson. *The Hydraulics of Open Channel Flow: An Introduction*. Elsevier, 1999.

[14] X. Chen and Y. Zong. Coastal erosion along the changjiang deltaic shoreline, china: History and prospective. *Estuarine, Coastal and Shelf Science*, 46:733–742, 1998.

[15] Jaepil Cho, Seungwoo Park, and Sangjun Im. Evaluation of agricultural nonpoin source (agnps) model for small watersheds in korea applying irregular cell delineation. *Agricutural Water Management*, 95:400–408, 2008.

[16] General Sciences Corporation. *SWRRBWQ Windows Interface User's Guide*. Office of Science and Technology, Standards and Applied Science Division, U.S. Environmental Protection Agency, Laurel, MD, 1993.

[17] Richarde Marques da Silva, Celso A.G. Santos, and Alexandro Medeiros Silva. Predicting soil erosion and sediment yield in the tapacura catchment, brazil. *Journal of Urban and Evironmental & Engineering*, 8:75–82, 2014.

[18] M.J. Castro Diaz, E.D. Fernandez-Nieto, and A.m. Ferreiro. Sediment transport models in shallow water equations and numerical approach by high order finite volume methods. *Computers & fluids*, 37:299–316, 2008.

[19] Nevena Dragicevic. *Model for erosion intensity and sediment production assessment based on erosion potential method modification - Doctoral Thesis*. Rijeka, 2016.

[20] Nevena Dragicevic, Barbara Karleusa, and Nevenka Ozanic. A review of the gavrilovic method (erosion potential method) application. *Gradevinar*, 68:715–725, 2016.

[21] Julie E.Laity. *Geomorphology of Desert Environments*. London, 1994.

[22] A. Folly, J.N. Quinton, and R.E. Smith. Evaluation of the eurosem model using data fro the catsop watershed, the netherlands. *Catena*, 37, 1999.

[23] G. Garegnani, G. Rosatti, and L. Bonaventura. On the range of validity of the Exner-based models for mobile-bed river flow simulations. *Journal of Hydraulic Research*, 51:380–391, 2013.

[24] L. Globevnik, D. Holjevic, G. Petkovsek, and J. Rubinic. Applicability of the gavrilovic method in erosion calculation using spatial data manipulation techniques. *IAHS*, 279, 2003.

[25] E.S. Gross, L. Bonaventura, and G. Rosatti. Consistency with continuity in conservative advection schemes for free-surface models. *International Journal of Numerical Methods in Fluids*, 38:307–327, 2002.

[26] N. Haregeweyn and F. Yohannes. Testing and evaluation of the agricultural non-point source pollution model (agnps) on augucho catchment, western hararghe, ethiopia. *Agricuture Ecosystems & Environment*, 99:201–212, 2002.

[27] S.P. Leatherman K. Zhang, B.C. Douglas. Global warming and coastal erosion. *Climatic change*, 1:41–58, 2004.

[28] National Soil Erosion Research Laboratory. *USDA-Water Erosion Prediction Project (WEPP).* US Department of Agriculture, West Lafayette, IN, 1995.

[29] H. Lantuit and W.H. Pollard. Fifty years of coastal erosion and retrogressive thaw slump activity on herschel island, southern beaufor sea, yukon territory, canada. *Geomorphology*, 95:84–102, 2008.

[30] D.M. Lawler, J.R. Grove, J.S. Couperthwaite, and J.L. Leeks. Downstream change in river bank erosion rates in the swale-ouse system, northern england. *Hydrological Processes*, 13:977–992, 1999.

[31] Stephen P. Leatherman, Keqi Zhang, and Bruce C. Boudglas. Sea level rise shown to drive coastal erosion. *EOS*, 81:55–57, 2000.

[32] Saro Lee. Soil erosion assessment and its verification using the universal soil loss equation and geographic information system: a case study at boun, korea. *Environmental Geology*, 45:457–465, 2003.

[33] J.C. Mars and D.W. Houseknecht. Quantitative remote sensing study indicates doubling of coastal erosion rate in past 50 yr along a segment of the arctic coast of alaska. *Geology*, 35:583–586, 2007.

[34] J.A. Martinez-Casasnovas. A spatial technology approach for the mapping and quantification of gully erosion. *Catena*, 50:293–308, 2003.

[35] W.S. Merritt, R.A. Letchera, and A.J. Jakeman. A review of erosion and sediment transport models. *Environmental Modelling & Software*, 18:761–799, 2003.

[36] M.E. Miller, M.A. Bowker, R.L. Reynolds, and H.L.Goldstein. Post-fire land treatments and wind erosion - lessons from the milford flat fire, ut, usa. *Aeolian Research*, 7:29–44, 2012.

[37] H. Mohammed, F. Yohannes, and G. Zeleke. Validation of agricultural non-point source (agnps) pollution model in kori watershed, south wollo, ethiopia. *Applied Earth Observation and Geoinformation*, 6:97–109, 2004.

[38] R.P.C. Morgan, J.N. Quinton, R.E. Smith, G. Poesen, J.W.A. Auerswald, K. Chisci, D. Torri, M.E. Styczen, and A.J.V. Folly. *The European Soil Erosion Model (EUROSEM).* Silsoe College, Cranfield University, Silsoe, Bedford, 1998.

[39] R.P.C. Morgan, J.N. Quinton, R.E. Smith, G. Poesen, J.W.A. Auerswald, K. Chisci, D. Torri, M.E. Styczen, and R.E. Smith. The european soil erosion model (eurosem): A dynamic approach for predicting sediment transport from fields and small catchments. *Earth Surface Processes and Landforms*, 23:527–544, 1998.

[40] N. Nagata, T. Hosoda, and Y. Muramoto. Numerical analysis of river channel processes with bank erosion. *Journal of Hyrdaulic Engineering*, 126:243–252, 2000.

[41] Karl F. Nordstrom and Shintaro Hotta. Wind erosion from cropland in the usa: a review of problems, solutions and prospects. *Geoderma*, 121:157–167, 2004.

[42] A. Pandey, V.M. Chowdary, B.C. Mal, and M. Billib. Runoff and sediment yield modeling from a small agricultural watershed in india using the wepp model. *Journal of Hydrology*, 348:305–319, 2008.

[43] G.P. Pennati, M. Bonasoro, S.B. Menajovsky, and G.C. Rossi. Enhanced snow-cover classification in satelite images using gis data. *Societe Francaise de Photogrammetrie et Teledetection*, 129, 1993.

[44] L. Pieri, M. Bitelli, J.Q. Wu, S. Dun, D.C. Flanagan, P.R. Pisa, F. Ventura, and F. Salvatorelli. Using the water erosion prediction project (wepp) model to simulate field-observed runoff and erosion in the apennines mountain range, italy. *Jounral of Hydrology*, 336:84–97, 2007.

[45] J. Poesen, J.Nachtergaele, G. Verstraeten, and C. Valentin. Gully erosion and environmental change: importance and research needs. *Catena*, 50:91–133, 2003.

[46] G. Rauws and G. Govers. Hydraulical and soil mechanical aspects of rill generation on agriculutral soils. *Journal of Soil Science*, 39:111–124, 1988.

[47] K.G. Renard, G.R. Foster, G.A. Weesies, D.K. McCool, and D.C. Yoder. *Predicting soil erosion by water: A guide to conservation planning with the Revised Universal Soil Loss Equation (RUSLE).* Agriculture Research Service, United States Department of Agriculture, Hyattsville, Maryland, 1997.

[48] K.G. Renard, G.R. Foster, D.C. Yoder, and D.K. McCool. Rusle revisited: Status, questions, answers and the future. *Journal of Soil and Water Conservation*, 49:213–200, 1994.

[49] D. Rickenmann. An alternative equation for the mean velocity in gravel-bed rivers and mountain torrents. *Hydraulic Engineering*, 1:672–676, 1994.

[50] A.P.J. De Roo, R.J.E. Offermans, and N.H.D.T. Cremens. Lisem: A single-event physically based hydrological and soil erosion model for drainage basins. ii: Sensitivity analysis, validation and application. *Hydrological Processes*, 10:1119–1126, 1996.

[51] A.P.J. De Roo and V.G.Jetten. Calibrating and validating the lisem model for two data sers from the netherlands and south africa. *CATENA*, 37:477–493, 1999.

[52] A.P.J. De Roo and C.G. Wesseling. Lisem: A single-event physically based hydrological and soil erosion model for drainage basins. i: Theory, input and output. *Hydrological Processes*, 10:1107–1117, 1996.

[53] B. Soto and F. Diaz-Fierros. Runoff and soil erosion from areas of burnt scrub: comparison of exmperimental results with those predicted by the wepp model. *Catena*, 31:257–270, 1997.

[54] Kenneth E. Spaeth, Frederick B. Pierson, Mark A. Weltz, and Wilbert H. Blackburn. Evaluation of usle and rusle esitmated soil loss on rangeland. *Journal of Range Management*, 56:234–246, 2003.

[55] S. Tanner, I. Katra, A. Haim, and E. Zaady. Short-term soil loss by eolian erosion in response to different rain-fed agricultural practices. *Soil and Tilleage Research*, 155:149–156, 2016.

[56] O. Terranova, L. Antronico, R. Coscarelli, and P. Iaquinta. Soil erosion risk scenarios in the Mediterranean environment using RUSLE and GIS: an application model for Calabria (southern Italy). *Geomorphology*, 112:228–245, 2009.

[57] U. Thampanya, J.E. Vermaat, S. Sinsakul, and N. Panapitukkul. Coastal erosion and mangrove progradation of southern thailand. *Estaurine Coastal and Shelf Science*, 68:75–85, 2006.

[58] Neil R. Viney and Murugesu Sivapalan. A conceptual model of sediment transport: application to the avon river basin in western australia. *Hydrological Processes*, 13:727–743, 1999.

[59] Sandra J. Winterbottom and David J. Gilvear. A gis-based approach to mapping probabilities of river bank erosion: regulated river tummel, scotland. *Regulated Rivers Resource Management*, 16:127–140, 2000.

[60] Walter H. Wischmeier and Dwight D. Smith. *Predicting rainfall erosion losses - A guide to conservation planning*. Science and Education Administration, United States Department of Agriculture, Hyattsville, Maryland, 1978.

[61] Saleh Yousefi, Nasrollah Moradi Kivarz, Bahar Ramezani, Niloofar Rasoolzadeh, Nastaran Naderi, and Somayeh Mirzaee. An estimation of sediment by using erosion potential method and geographic information systems in chamgardalan watershed: A case study of ilam province, iran. *Geodynamics Research International Bulletin*, 2:34–41, 2014.